Sedimentary record of a Late Cretaceous volcanic arc in central Patagonia: petrography, geochemistry and provenance of fluvial volcaniclastic deposits of the Bajo Barreal Formation, San Jorge Basin, Argentina

Aldo M. Umazano [a,*], Eduardo S. Bellosi [b], Graciela Visconti [c], Guillermo A. Jalfin [d], Ricardo N. Melchor [a]

[a] Consejo Nacional de Investigaciones Científicas y Técnicas and Facultad de Ciencias Exactas y Naturales, Universidad Nacional de La Pampa.
Av. Uruguay 151, 6300 Santa Rosa, La Pampa, Argentina
[b] Consejo Nacional de Investigaciones Científicas y Técnicas and Museo Argentino de Ciencias Naturales. Av. Ángel Gallardo 470, 1405 Buenos Aires, Argentina
[c] Facultad de Ciencias Exactas y Naturales, Universidad Nacional de La Pampa. Av. Uruguay 151, 6300 Santa Rosa, La Pampa, Argentina
[d] IPM, Schlumberger. Schlumberger House, Buckingham Gate, Gatwick Airport, RH6 0NZ, UK

A R T I C L E   I N F O

A B S T R A C T

The Upper Cretaceous Bajo Barreal Formation (San Jorge Basin, Argentina) is a fluvial succession mostly composed of channel sandstones interbedded with thicker floodplain deposits dominated by tuffaceous strata. The goal of this contribution is to infer the provenance of the unit through combined petrographical and geochemical data of channel sandstones, primary tuffs and tuffo-psammites (reworked, no-mixed tuffs). Channel sandstones are dominantly litharenites and feldspathic litharenites with abundant participation of volcanic lithic fragments with different textures (porphyritic, eutaxitic, felsitic, pilotaxitic, trachytic and vitric-vitrophyric), pumice and plagioclase. K-feldspar, quartz and sedimentary rock fragments are scarce. QFLu diagram and several provenance indicators including dominance and textural types of rock fragments, K-feldspar/plagioclase ratio and inclusion-free quartz grains indicate a provenance from felsic to intermediate, pyroclastic-rich, arc-related volcanic rocks. This interpretation agrees with the values of various elemental ratios of trace elements such as La/Sc, Th/Sc, Cr/Th, Eu/Eu* and (La/Lu)$_N$ and discriminant functions based on major elements.

Pyroclastic floodplain strata are commonly pumice-rich, occasionally glass shard-rich, vitric tuffs suggesting an origin from plinian-like eruptions. Subordinate components include volcanic lithic fragments, quartz, orthoclase and plagioclase. Zr/Ti versus Nb/Y and SiO$_2$ versus K$_2$O diagrams, as well as a multi-element diagram of selected trace elements shows that the pyroclastic rocks were originated from medium-K content, intermediate, arc related magmatic source.

Considering the palaeoflow direction towards the east and south-east and presence of subduction processes along the western margin of Patagonia during the Late Cretaceous, it is interpreted that Bajo Barreal Formation constitutes the sedimentary record (distal facies of volcano-flanking fan or apron) of this coeval volcanic arc. Channel sandstones probably were mostly derived from the Divisadero Formation volcanic rocks because of similar petrographical features and REE pattern. In contrast, pyroclastic tuffaceous floodplain deposits would be derived from vents located over the actual outcrops of the Patagonian Batholith.

1. Introduction

The Upper Cretaceous Bajo Barreal Formation and laterally equivalent lithostratigraphic units of the Chubut Group bear the main hydrocarbon reservoirs in the subsurface of the San Jorge Basin, central Patagonia, Argentina (Feruglio, 1949; Lesta, 1968; Sciutto, 1981; Fitzgerald et al., 1990). The sedimentary succession of the Bajo Barreal Formation is typically composed of fluvial channel-fill volcaniclastic sandstones interbedded with thicker and finer-grained floodplain deposits dominated by tuffaceous strata and ash-fall tuffs (Sciutto, 1981; Bridge et al., 2000; Umazano et al., 2008). Petrographic studies of the sandstone bodies of the Bajo Barreal Formation and equivalents both from outcrop samples (Teruggi, 1962; Teruggi and Rosetto, 1963; Davies et al., 1994; Tunik et al., 2004; Umazano et al., 2006) and well cores (Dunn and Surdam, 1992; Tófalo et al., 1992; Estrada,

* Corresponding author.
  E-mail address: amumazano@exactas.unlpam.edu.ar (A.M. Umazano).

2002; Gonzalez et al., 2002; Salomone et al., 2002; Sanagua et al., 2002) focused on its characterization as reservoir rocks. These studies emphasized the high content of volcanic lithic fragments and plagioclase, as well as the subordinate presence of K-feldspar and quartz. A preliminary study of sandstone detrital modes of the Chubut Group only included three samples from the Bajo Barreal Formation, suggesting an undissected-transitional arc provenance from a western source without further details (Tunik et al., 2004). On the other hand, petrographic and geochemical studies of the associated pyroclastic floodplain deposits of the Bajo Barreal Formation are unknown. In consequence, although a derivation from a western source was speculated many years ago beginnings with the pioneering work by Feruglio (1949), there are no studies that confirm this supposition. In addition, the characterisation of the volcanism, the probable location of the source vents, and a definite correlation with source rocks remain unknown.

According to the palaeogeographic configuration of central Patagonia and the regional geology, potential source areas for sediments of the Bajo Barreal Formation include: *i*) Protero-zoic-Palaeozoic metamorphic, sedimentary and igneous rocks of the Deseado Massif, to the south of the basin; *ii*) Early Jurassic-Middle Jurassic silicic volcanic rocks of the Chon Aike province from the Nordpatagonian and Deseado massifs (Lesta and Ferello, 1972; Pankhurst et al., 1998); *iii*) Late Cretaceous plutonic rocks of the Patagonian Batholith located along the Argentina-Chile border (Pankhurst et al., 1999; Hervé et al., 2007) and the related back-arc volcanic rocks (Parada et al., 2001). The goal of this contribution is to infer the provenance of the Bajo Barreal Formation channel sandstones and associated floodplain deposits using detailed petrographic and geochemical data within a well-established stratigraphic and lithofacies scheme.

2. San Jorge Basin: stratigraphy and tectonic setting

The San Jorge Basin is located in central Patagonia covering the southern sector of the Chubut province and the northern sector of the Santa Cruz province, Argentina (Fig. 1). The basin boundaries are the Nordpatagonian Massif and Cañadón Asfalto Basin to the north, the Deseado Massif to the south, the Patagonian Andes to the west and the continental margin of the Atlantic Ocean to the east. It is an extensional intracontinental trough developed on Palaeozoic continental crust, and linked to the break-up of Gondwana and opening of the South Atlantic Ocean during Jurassic times (Barcat et al., 1989; Fitzgerald et al., 1990). The basin was filled with pyroclastic and epiclastic sediments since the Jurassic to the Miocene (Fig. 2). Initially, a volcanic-sedimentary complex of Middle Jurassic age assigned to the Bahía Laura or Lonco Trapial groups was deposited in NW-SE trending half-grabens (Lesta and Ferello, 1972). The Late Jurassic-Late Cretaceous succession is divided into two groups or megasequences. The lower is the Las Heras Group (Malm-Hauterivian), which represent lacustrine sedimentation with Pacific marine influence in discontinuous depocentres corresponding to grabens and half-grabens during synrift conditions (Figari et al., 1999).

The upper megasequence is much more extended and corre-sponds to the Chubut Group (Barremian-Maastrichtian), which overlies the Lonco Trapial and Las Heras groups, confirming the asymmetrical filling of a basin elongated in W-E direction (Jalfin et al., 2002). Fitzgerald et al. (1990) suggested that this mega-sequence was deposited during a sag stage; whereas Figari et al. (1999) considered that represent a new rifting event. The sedi-mentary succession of the Chubut Group is composed of continental sediments with abundant input of primary volcaniclastic material. The Chubut Group crops out along the San Bernardo Range (Fig. 1), a fold belt with a NNW-SSE orientation formed by compresional
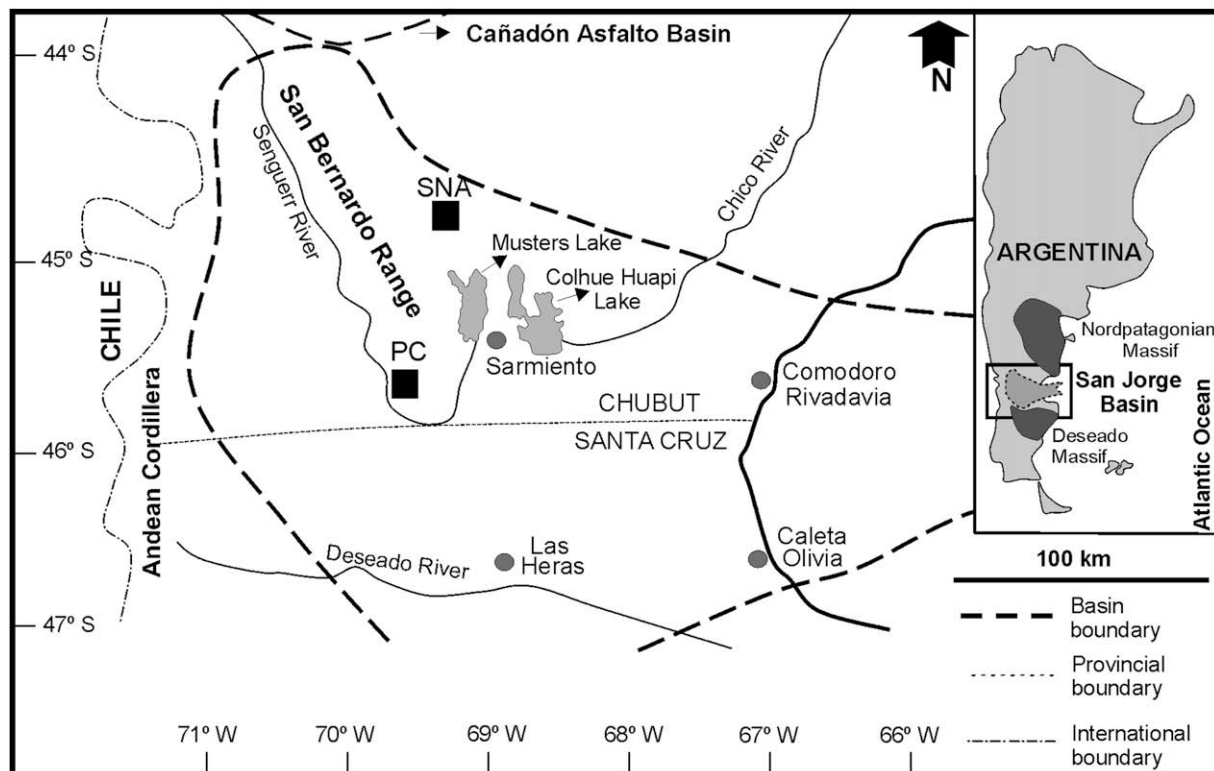

Fig. 1. Location map for the San Jorge Basin, central Patagonia, Argentina. The studied localities are: Puesto Confluencia (PC) and Sierra Nevada Anticline (SNA).
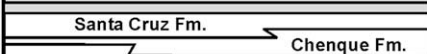
Fig. 2. Stratigraphic chart for the western sector of the San Jorge Basin (after Umazano et al., 2008). The zig-zag lines mark partially synchronous litostratigraphic units.

efforts linked to Neogene Andean tectonism (Peroni et al., 1995). At the San Bernardo Range, the Chubut Group is composed of a succession of sediments arranged in five units approximately 2.000 m thick, in ascending order: the D-129, Matasiete, Castillo, Bajo Barreal and Laguna Palacios formations (Fig. 2). The D-129 Formation includes organic-rich lacustrine and marginal lacustrine sediments, which is the main hydrocarbon source rock of the basin (Uliana et al., 1999), whereas the overlying formations act as reservoirs (Jalfin et al., 2005). At the basin margin, the coastal lacustrine facies are replaced by fluvial deposits of the Matasiete Formation (Paredes et al., 2003, 2007). The overlying Castillo and Bajo Barreal formations were deposited in fluvial to lacustrine environments, accompanied by a more voluminous input of tephra (Sciutto, 1981; Bridge et al., 2000; Umazano et al., 2008). The sedimentary succession of the Bajo Barreal Formation can be divided in two members: *i*) a lower member mainly composed of laterally continuous primary and reworked tuff beds interbedded with lenses of sandstones and *ii*) an upper member dominated by tuffaceous siltstones with subordinated sandstone lenses and very scarce primary tuff beds (Sciutto, 1981). According to Umazano et al. (2008) the lower member records sedimentation in a braided fluvial system with important discharge variations and abundant ash-fall events (see also Archangelsky et al., 1994; Bridge et al., 2000), whereas the upper member represents sedimentation in a fluvio-aeolian system with high a loessic input. The upper unit of the Chubut Group is the Laguna Palacios Formation, a tuffaceous loess-palaeosol succession, which records the final terrestrial sedimentation in the San Jorge Basin periphery (Bellosi and Sciutto, 2002; Genise et al., 2002). Field relationships suggest that the upper section of the Bajo Barreal and the Laguna Palacios formations are laterally correlative and partially synchronous (Sciutto, 1981).

Two episodes of Atlantic marine transgressions occurred since Maastrichtian times that resulted in deposition alternating between marine (Salamanca and Chenque formations) and continental sediments (Río Chico Group and Sarmiento and Santa Cruz formations) in the basin (Legarreta and Uliana, 1994; Bellosi, 1995).

3. Patagonian Andes

The western boundary of the San Jorge Basin are the Patagonian Andes (Fig. 3), which run along the Argentina-Chile border between latitude 38°S and 55°S. This cordillera began to form in the Mesozoic as a result of both eastward subduction of a series of Pacific oceanic plates and the absolute motion of the South American Plate to the west since the opening of the South Atlantic Ocean (Folguera and Ramos, 2002).

The Patagonian Andes are formed by: *i*) a Late Palaeozoic-Mesozoic (?) metamorphic complex, *ii*) the Late Jurassic-Pleistocene Patagonian Bathotith and *iii*) Late Jurassic-Tertiary back-arc volcanic and sedimentary rocks (Fig. 3). The oldest units are fore-arc sedimentary rocks accreted and metamorphosed during subduction beneath southwestern Gondwana. The Patagonian Batholith is mostly composed of granodioritic plutons typically metaluminous and calc-alkaline, emplaced during episodic magmatism (Pankhurst et al., 1999). The Liquiñe-Ofqui Fault Zone (LOFZ, Fig. 3), a fault system that runs along the axis of the Patagonian Batholith, controls the location of the active volcanoes (Cembrano et al., 1996). Towards the east of the Patagonian Batholith, the back-arc volcanic rocks and their sedimentary intercalations are widely distributed and have received diverse denominations in different geographic regions. In this paper, we follow the stratigraphic framework outlined by Parada et al. (2001) for the Aysén region (Chile) because of its detailed geochronologic control.

During the Late Jurassic, the acid back-arc volcanism resulted in rhyolitic tuff sequences recorded as the Ibañez Formation, which has been included within the Chon Aike large silicic igneous province (Pankhurst et al., 1998). However, further east in Argentina, Ramos (1976) described andesitic lavas and tuffs as the main constituents of the equivalent La Plata Formation. The Cretaceous volcanism is represented by volcanic rocks of the Divisadero and Ñirehuao formations. Several radiometric ages of both units indicate that the volcanic activity took place during the Albian-Campanian with an apparent climax in the Cenomanian-Campanian (Parada et al., 2001), approximately coeval with the deposition of the Bajo Barreal Formation in the San Jorge Basin (Archangelsky et al., 1994; Bridge et al., 2000). The Cretaceous back-arc volcanism is characterized by a bimodal association of abundant tuffs and lavas of rhyolithic and dacitic composition, and a minor amount of basaltic and andesitic lavas. Although the Ñirehuao Formation is lithologically similar to the Divisadero Formation, it contains a larger amount of basaltic rocks (Parada et al., 2001). Tertiary back-arc volcanic events are represented by the Chile Chico Formation and several Eocene-Pliocene sequences of flood basalts (Parada et al., 2001; Ramos and Kay, 1992).

4. Study area

This study was carried out in two localities of the San Bernardo Range, called Puesto Confluencia (PC) and Sierra Nevada Anticline (SNA), both in the Chubut province and located approximately 68 km apart (Fig. 1). PC (45° 43′ 33″ S; 69° 41′ 11″ W) is located on the left margin of the Senguerr River, at the southwestern flank of the San Bernardo Range. At this locality, the Bajo Barreal Formation is 450 m thick and dips 5° to SW, composing the western limb of a faulted anticline with an axial trace orientated approximately N-S. The second section of the Bajo Barreal Formation is 176 m thick and was measured in the eastern limb of the SNA (44° 50′ 50″ S; 69° 25′

21″ W), where the strata dip 10° to NE. This anticline is an asymmetrical structure with an NW-SE axial trace and northward plunge. Fig. 4 shows simplified sedimentary logs of the Bajo Barreal Formation for both localities (after Umazano et al., 2008).

5. Methods

Samples for petrographic studies and geochemical analyses included both channel sandstones and floodplain pyroclastic rocks (Fig. 4). The later include primary ash-fall tuffs and reworked tuffs that lack epiclastic components (tuffo-psammites sensu Teruggi et al., 1978). Twenty three sandstone thin sections (sixteen from PC and seven from SNA) and fifteen pyroclastic thin sections (seven from PC and eight from SNA) were analyzed using a Nikon petrographic microscope. Four hundred points per thin section were counted (clasts, matrix, cement and porosity) using a Model G Prior point-counter. Roundness and sphericity was estimated by visual comparison (Powers, 1953). Porosity was classified according to Boggs (1992). For estimation of modal composition of sandstones, the Gazzi-Dickinson point-counting method (Ingersoll et al., 1984) was followed. Additionally, each rock fragment that contains crystals ≥0.0625 mm was also computed for use in the Folk et al. (1970) classification scheme. Plagioclase composition was estimated using the Michel-Lévy optical method (Rogers and Kerr,

1942). Differentiation of zeolitic minerals was realized by optical criterions. For distinction of petrofacies, cluster analysis using the group average method and squared Euclidean distance was made by means of Statgraphics program.

Forty samples including twenty five sandstones (twenty from PC and five from SNA) and fifteen tuffs or tuffo-psammites (seven from PC and eight from SNA) were selected for geochemical analysis. Bulk rock analysis of major and trace elements were determined by Actlabs Laboratories. Major oxide compositions and some trace elements (Sc, Be, V, Sr, Zr and Ba) were determined using the inductively coupled plasma optical emission spectrometry technique (ICP). The remaining trace elements were determined using the inductively coupled mass spectrometry method (ICP-MS). The Chemical Index of Alteration (CIA $= [Al_2O_3/(Al_2O_3 + CaO^* + Na_2O + K_2O)] \times 100$) was calculated after Nesbitt and Young (1982) for samples lacking carbonate cement.

6. Sandstone petrography and detrital modes

The samples from PC show framework grains that represent from 51% to 91.5% of the rock volume, scarce orthomatrix (0% to 2%) and variable proportions of cement (1% to 38.75%). SNA samples have framework grains that constitute from 63.25% to 82.75% of the rock volume, lack matrix, and the cement ranges from 14.75% to
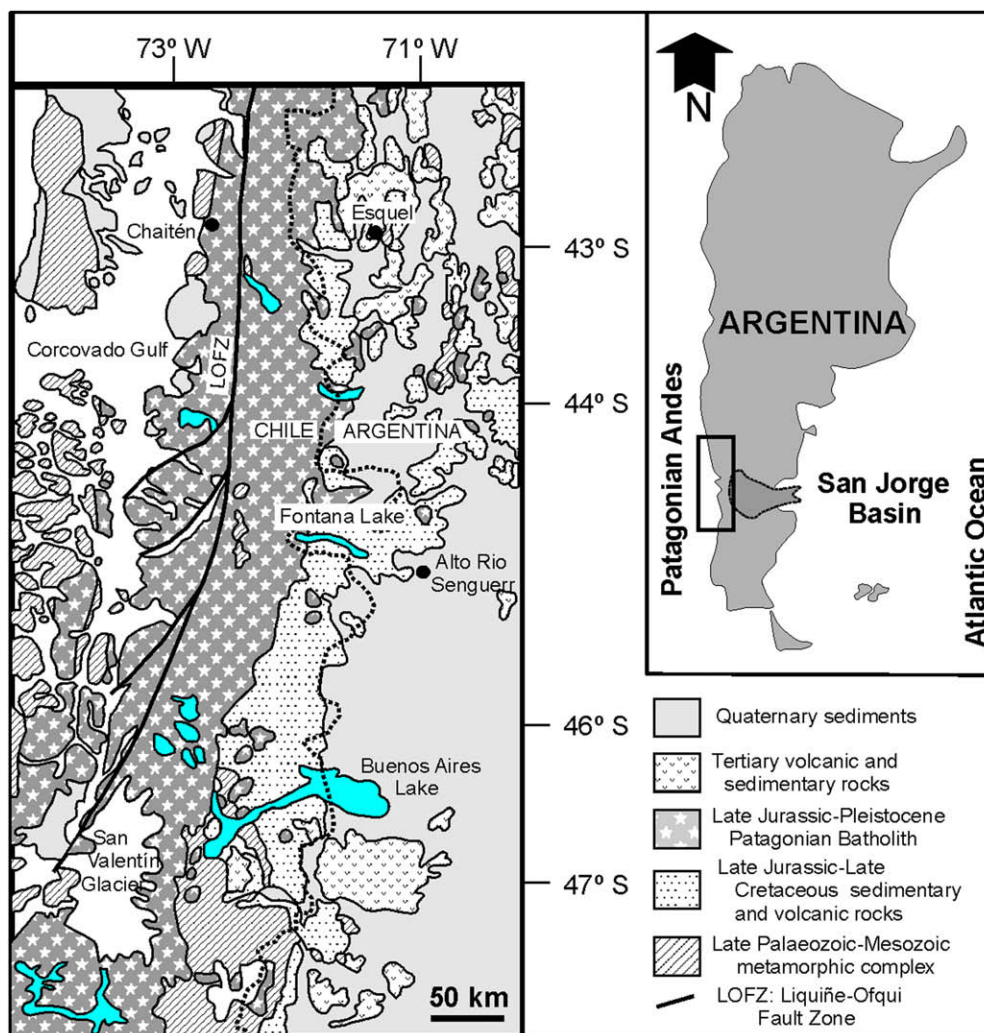
Fig. 3. Simplified geologic map of the Patagonian Andes between latitudes of 42°S and 48° S (after Parada et al., 2001; Rolando et al., 2002).
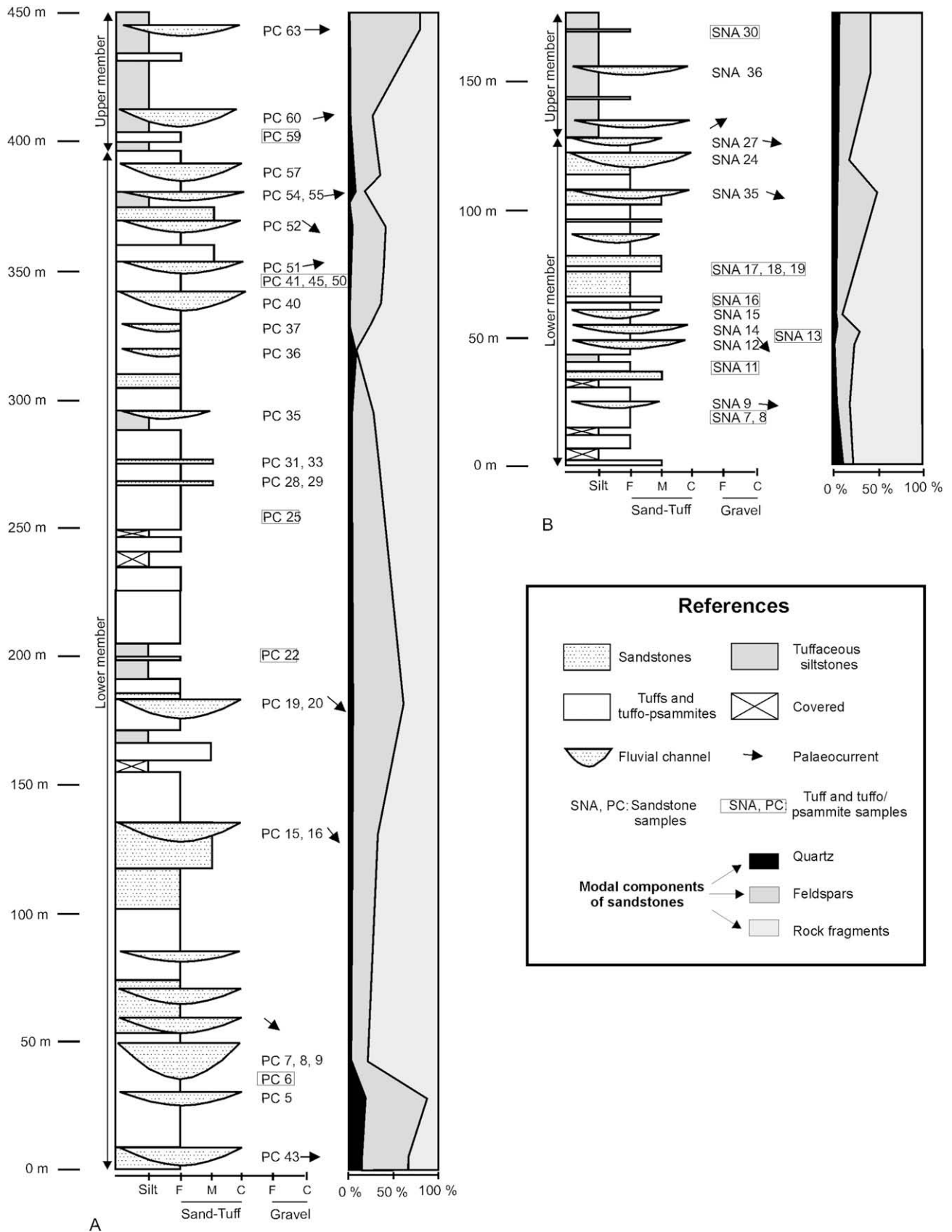
Fig. 4. Schematic sedimentary logs of the Bajo Barreal Formation at PC (A) and SNA (B), showing the location of the samples for petrographic and geochemical studies (modified from Umazano et al., 2008). The vertical distribution of modal components of the sandstones at both localities also is presented. The pyroclastic samples are enclosed by a panel.

36.75%. In both localities, samples are poorly to well sorted and the framework grains are sub-rounded to sub-angular with low sphericity. The clastic fraction displays open packing dominated by clast-supported grains with few tangential contacts, along with subordinate long and concave-convex contacts. Commonly, this fraction is composed in decreasing order of abundance by rock fragments, feldspars and quartz (Table 1, Fig. 4 and Fig. 5A). Only four samples from PC have a greater abundance of feldspars in relation to rock fragments (PC43, PC5, PC19 and PC63; Fig. 5B). The rock fragments are usually partially altered volcanic lithic grains, with different textures, and pumice clasts. The more common textures recognized are: porphyritic (Lvp, plagioclase phenocrysts surrounded by a quartz-feldspathic groundmass), eutaxitic (Lve, amalgamated glass shards with subtle planar characteristics) and felsitic (Lvf, equigranular mosaic of quartz and feldspars). In minor proportion, pilotaxitic (Lvpi, unoriented plagioclase laths), trachytic (Lvt, feldspathic microlites of parallel disposition) and occasionally vitric-vitrophyric (Lvd, glass altered to feldspars and/or quartz forming spherulites) textures were also identified. Commonly, the volcanic lithic grains with different texture and pumice fragments (Pu) tend to occur in pairs as follows: Lvf and Lvp, Lvpi and Lvt, and Lve and Pu; Lvd generally occurs associated with Lvf or Lvp. Sedimentary rock fragments of intraclastic origin are very scarce.

The dominant feldspar is altered or fresh plagioclase crystals with common oscillatory zonation and twined according to albite, Carlsbad, pericline and Carlsbad-albite combined laws. The plagioclase composition varies from oligoclase to andesine. In relation to plagioclase, K-feldspar is less abundant and only

Table 1

Composition of sandstone framework grains from the Bajo Barreal Formation at PC and SNA localities. Qms: monocristalline quartz with straight extinction. Qmu: monocristalline quartz with undulose extinction. Qp: polycristalline quartz. Or: orthoclase. The plagioclases (P) are divided depending to the twin types (c: Carlsbad; a: albite; p: pericline) and presence of zonation (z). The volcanic lithic fragments (Lv) are distinguished according to their textures: felsitic (Lvf), porphyritic (Lvp), trachytic (Lvt), pilotaxitic (Lvpi), eutaxitic (Lve) and vitric-vitrophyric (Lvd). Pu: pumice fragment. Ls: sedimentary rock fragment. Amp: amphibole. Px: pyroxene. Mc: mica. Op: opaque mineral. Alt: alterites

Sample #	Quartz (%)											Feldspars (%)								
	Qmu	Qms	Qp	Or	Pc	Pa	Pca	Pp	Pz	Pzc	Pza	Pzp	Pn	Pzn	Pap	Papz	Pcp	Pcaz	Pcap	Pcapz
Pc 43	–	13.97	–	24.25	4.8	11.35	6.55	–	–	3.5	1.31	1.74	0.87	–	–	–	–	–	–	–
Pc 5	5.88	10.29	0.49	26.47	3.92	18.13	6.86	1.96	4.41	1.47	2.94	–	0.98	–	0.98	–	–	–	–	–
Pc 7	–	2.53	–	12.99	0.72	17.69	5.77	1.44	–	1.8	1.8	0.36	0.36	–	0.36	–	–	0.36	–	–
Pc 15	1.59	2.86	–	6.03	2.22	9.52	2.54	1.59	0.63	0.32	0.63	–	1.59	–	1.27	–	–	–	0.32	–
Pc 19	–	4.83	–	11.73	2.75	10.69	11.72	4.48	2.41	0.34	2.41	–	3.44	2.06	2.41	1.03	0.69	–	–	–
Pc 31	–	2.19	–	7.65	1.09	5.19	3.28	–	4.92	1.64	3	1.64	1.91	–	1.91	–	1.09	0.55	–	–
Pc 35	–	3.82	–	11.17	2.06	3.53	1.76	0.58	2.64	–	–	–	4.11	–	–	–	–	–	–	–
Pc 36	1.7	4.08	–	3.74	2.04	4.08	4.42	0.34	1.7	0.68	4.76	–	4.08	1.02	-	0.34	–	0.34	–	0.68
Pc 37	–	6.23	–	2.93	4.03	7.33	2.2	–	0.73	–	1.1	–	0.37	–	–	–	–	–	–	0.37
Pc 40	–	1.11	–	4.8	2.58	4.06	5.17	0.37	7.01	1.85	2.95	–	3.32	–	1.11	–	0.37	–	–	0.37
Pc 51	0.81	0.81	–	7.29	1.61	8.9	2.43	2.02	1.21	0.8	3.24	–	2.43	1.21	1.61	–	–	–	0.81	–
Pc 52	–	3.28	–	6.2	3.28	5.47	5.47	1.09	3.28	1.45	1.45	–	2.92	–	1.09	–	–	0.36	–	–
Pc 54	–	–	–	2.61	5.22	–	2.61	–	1.87	1.87	1.12	–	2.61	0.75	1.12	–	–	–	–	–
Pc 55	–	6.45	0.36	8.6	9.32	0.36	2.15	–	1.8	–	2.15	–	2.51	–	–	–	0.72	–	–	–
Pc 60	–	1.14	–	6.44	3.41	7.57	4.55	–	0.38	–	–	–	2.28	–	–	–	0.38	–	0.76	–
Pc 63	–	2.33	–	15.95	2.73	10.51	12.84	7.4	5.45	0.78	5.83	3.9	4.28	0.39	4.67	–	–	–	–	–
Sna 9	–	2.72	–	4.53	3.32	1.81	2.11	0.3	0.3	–	–	–	1.81	–	–	–	0.3	–	–	–
Sna 12	–	1.01	–	7.09	3.04	5.4	3.71	0.68	0.34	0.34	0.34	–	2.37	–	0.34	–	0.34	–	–	–
Sna 14	0.79	2.77	–	6.72	1.98	5.44	3.96	1.19	1.59	–	0.4	0.4	0.79	–	0.4	–	–	–	–	–
Sna 15	–	2.14	–	1.42	1.42	1.07	1.78	–	1.42	–	–	–	0.72	–	–	–	–	–	–	–
Sna 35	–	3.63	0.66	3.63	2.64	3.3	2.31	–	1.65	0.33	–	–	1.65	–	–	–	–	–	–	–
Sna24	0.93	3.4	–	7.72	5.25	6.17	4.94	2.46	2.47	0.93	1.24	–	2.47	–	–	–	1.24	–	0.93	0.31
Sna 36	0.34	2.36	–	9.8	6.09	7.1	7.77	–	3.38	0.34	–	–	3.37	–	0.34	–	0.34	–	–	–

| Sample #	Rock fragments (%)								Accesory minerals (%)				Alt. (%)	Total
	Lvf	Lvp	Lvt	Lvpi	Lve	Lvd	Pu	Ls	Amp	Px	Mc	Op		
Pc 43	7.86	10.04	–	0.44	0.87	9.17	0.87	–	–	–	–	1.31	0.87	100
Pc 5	7.84	4.9	–	–	–	–	0.98	–	–	–	–	1.47	–	100
Pc 7	7.59	40.44	–	–	1.44	3.97	–	–	0.36	–	–	–	–	100
Pc 15	1.9	11.75	–	6.03	9.2	2.22	27.3	–	–	–	–	3.49	6.98	100
Pc 19	4.82	9.31	5.17	7.24	5.52	1.38	2.07	–	–	–	–	–	3.45	100
Pc 31	3.83	10.65	4.92	0.82	2.46	0.27	33.88	–	–	0.27	–	0.82	6.01	100
Pc 35	2.35	3.82	-	0.59	28.82	1.47	26.76	–	–	–	0.29	–	5.88	100
Pc 36	9.18	14.63	7.14	3.74	19.05	0.68	6.8	–	–	–	–	–	3.74	100
Pc 37	6.96	17.95	28.57	9.52	1.1	6.96	–	–	–	–	–	–	2.2	100
Pc 40	11.81	4.43	2.58	1.11	16.61	–	22.51	–	0.37	–	0.37	0.37	4.06	100
Pc 51	2.43	14.97	3.24	–	8.91	1.62	26.32	–	–	–	1.21	1.62	4.45	100
Pc 52	9.49	15.33	1.82	0.36	2.19	1.46	18.61	–	0.36	–	1.09	–	11.31	100
Pc 54	14.55	29.85	10.44	12.31	1.49	2.99	3.36	2.24	0.37	–	–	–	0.75	100
Pc 55	2.51	7.53	3.23	6.09	4.3	–	30.11	–	–	–	–	2.15	9.68	100
Pc 60	6.82	19.32	10.61	1.52	14.77	–	15.91	–	–	–	–	1.14	3.03	100
Pc 63	5.45	5.06	2.33	0.39	2.33	–	5.06	–	–	–	0.39	–	0.39	100
Sna 9	2.11	8.16	1.51	2.42	6.34	–	54.68	–	0.3	0.3	1.81	–	5.14	100
Sna 12	2.03	19.26	5.41	4.73	7.77	3.38	27.7	0.34	–	–	–	1.35	3.04	100
Sna 14	3.95	3.56	2.77	10.28	5.93	0.79	32.41	–	0.79	–	1.19	0.79	11.07	100
Sna 15	2.85	4.63	4.62	2.14	29.54	–	36.3	–	–	–	0.36	0.36	9.25	100
Sna 35	5.28	4.95	1.22	2.31	18.15	–	44.22	–	–	0.33	0.33	–	3.3	100
Sna 24	3.09	3.09	0.62	0.31	3.09	4.63	39.81	–	0.31	–	0.31	0.93	3.4	100
Sna 36	4.73	5.74	2.36	3.04	9.8	0.68	19.26	–	1.69	–	3.04	3.38	4.73	100
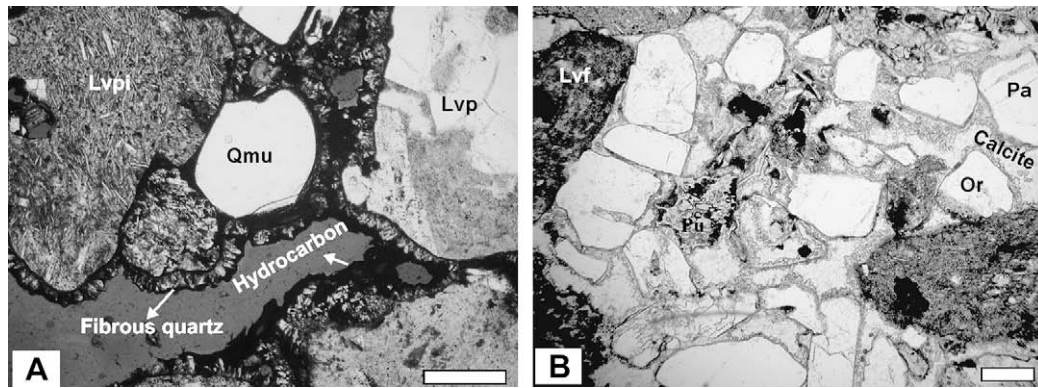
Fig. 5. Microphotographs of the Bajo Barreal Formation sandstones. A, general view of a litharenite (PC 37) showing monocrystalline quartz with undulate extinction (Qmu) and volcanic lithic fragments with pilotaxitic (Lvpi) and porphyritic (Lvp) textures; note the presence of fibrous quartz cement and partial hydrocarbon impregnation. B, general view of a lithic arkose (PC 43) showing crystals of plagioclase with albite twin (Pa) and orthoclase (Or), as well as pumice (Pu) and volcanic lithic fragments with felsitic texture (Lvf); cement is sparry calcite. Scale bars = 0.5 mm, parallel light.

represented by fresh orthoclase crystals. The quartz is generally inclusion-free fresh monocrystalline crystals with straight extinction, although scarce individuals with undulose extinction were detected. Policrystalline quartz is very scarce, always showing more than five subgrains. Accessory minerals are represented by hornblende, undetermined pyroxenes, biotite and opaque minerals.

The principal cement types are clay coatings and microgranular or fibrous quartz, although several samples show abundant zeolitic minerals (analcime and clinoptilolite) generally as partial to total replacement of framework grains, or scarce sparry calcite patches. At PC, the optical porosity ranges from 1.5% to 24.75%, with an average of 12.6%, and it is dominated by mesopores ($\overline{X} = 0.21$ mm, $n = 800$) with occasional oil impregnations (Fig. 5A). On the other hand, at SNA the mean optical porosity is 2.25% and ranges from 0% to 6.75%, and also appears as mesopores ($\overline{X} = 0.03$ mm, $n = 250$). In both localities, the porosity is mainly secondary, recorded by partial to total grain dissolution or fractures of rock fragments and plagioclase, though primary intergranular porosity occurs subordinately. The studied samples can be considered volcanic sandstones (Fisher, 1961) and mostly classified as feldspathic litharenites and litharenites (Folk et al., 1970; Fig. 6). Nevertheless, two

lithic arkoses and two feldsarenites samples from PC were identified. The average detrital modes are $Q_4F_{34}L_{62}$ and $Q_3F_{24}L_{73}$ for the sandstones of PC and SNA, respectively.

Cluster analysis of the absolute abundance of the volcanic lithic fragments and pumice clasts in sandstone detrital modes within the Bajo Barreal Formation allowed us to distinguish four petrofacies (rocks of similar petrology, sensu Dickinson and Rich, 1972), which were named V1 to V4 (Fig. 7). Petrofacies V1 (Lvf$_8$ Lvp$_{25}$ Lvt$_0$ Lvpi$_1$ Lve$_1$ Lvd$_7$ Pu$_1$) and V4 (Lvf$_{11}$ Lvp$_{24}$ Lvt$_{20}$ Lvpi$_{11}$ Lve$_1$ Lvd$_5$ Pu$_2$) have abundant participation of porphyritic and vitric-vitrophiric grains, as well as reduced amount of eutaxitic and pumice clasts. These petrofacies can be distinguished by the content of trachytic and pilotaxitic grains, which is very low in V1 and large in V4. In comparison, petrofacies V2 (Lvf$_8$ Lvp$_{11}$ Lvt$_4$ Lvpi$_1$ Lve$_9$ Lvd$_1$ Pu$_{12}$) and V3 (Lvf$_3$ Lvp$_8$ Lvt$_3$ Lvpi$_4$ Lve$_{11}$ Lvd$_1$ Pu$_{31}$) are enriched in eutaxitic and pumice grains, depleted in vitric-vitrophyric and porphyritic grains, whereas the content of trachytic and pilotaxitic grains is intermediate. Although pumice content is high in petrofacies V2 and V3, it is higher in petrofacies V3 than in petrofacies V2. All samples from SNA belong to the petrofacies V3. In contrast, the four petrofacies are represented in the samples from PC locality,
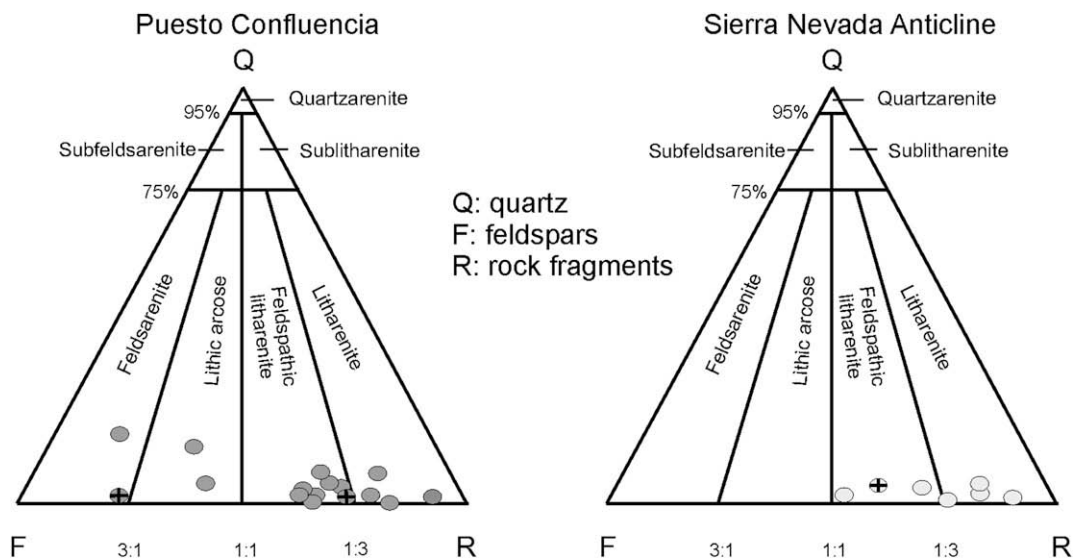

Fig. 6. Sandstone's classification diagrams according to Folk et al. (1970). The dark gray and ligth gray circles represent samples from PC and SNA, respectively. Those circles with cross belong to the upper member.
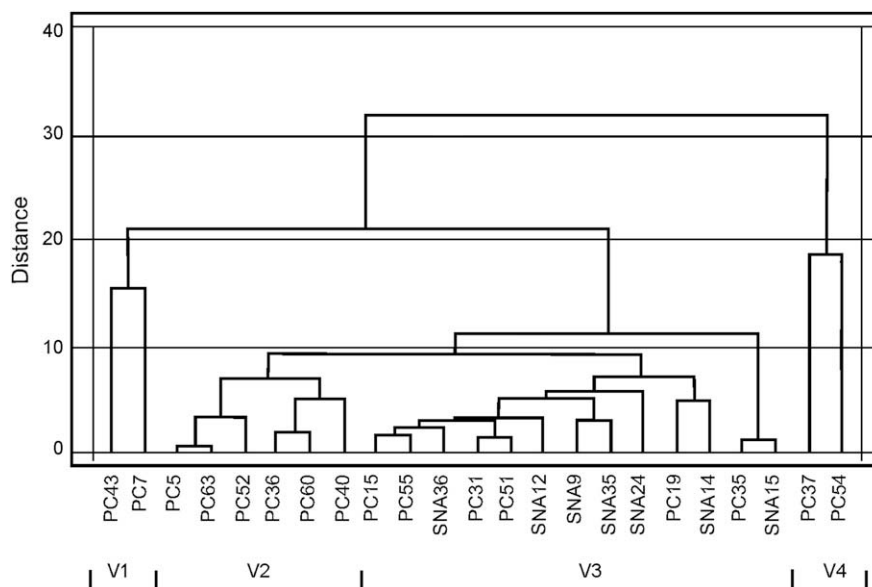
Fig. 7. Dendrogram showing the clustering of petrographic variables for the samples of the Bajo Barreal Formation. Cluster analysis was made using the group average method and squared Euclidean distance.

although in different proportion: V1 (12.5%), V2 (37.5%), V3 (37.5%) and V4 (12.5%). A preferred stratigraphic position of the different petrofacies was not detected.

The sandstone samples from the Bajo Barreal Formation plots in undissected-transitional arc provenance field, using the classic ternary provenance diagram of Dickinson et al. (1983, Fig. 8). Samples # PC5, PC43, SNA14 and SNA15 were excluded for the provenance analysis because of the amount of cement is higher than 25% (cf. Dickinson and Suczek, 1979).

7. Petrography of tuffs and tuffo-psammites

Thin section analysis revealed that pyroclastic samples from PC and SNA are very similar. They are commonly moderately well-sorted and have framework grains dominated by long contacts. The framework grains compose up to 85.5% and 74.75% of the rock volume at the northern and southern localities, respectively.

This fraction is dominated by fine-grained, sub-angular to angular, low-sphericity vitroclasts surrounding medium-grained, sub-rounded to sub-angular, low-sphericity lithoclasts or phenocrysts (Table 2; Fig. 9). The vitroclasts are replaced by zeolites and include cuspate or platy glass shards, pumice with flattened vesicles and pumice with rounded to ellipsoidal vesicles. Although pumice is the main vitric component, some pyroclastic layers are enriched in glass shards (samples # SNA8, SNA17, SNA19 and PC6). The phenocrysts commonly occur as euhedral and fresh grains including inclusion-free monocrystalline quartz with straight extinction, orthoclase and generally twined, occasionally oscillatory zoned plagioclase. Composition of plagioclase is mainly oligoclase to andesine. The more common lithoclasts are altered volcanic lithic fragments with felsitic and porphyritic textures; less commonly trachytic, pilotaxitic and eutaxitic textures also occur. In decreasing order of abundance, accessory minerals are represented by opaque minerals, biotite
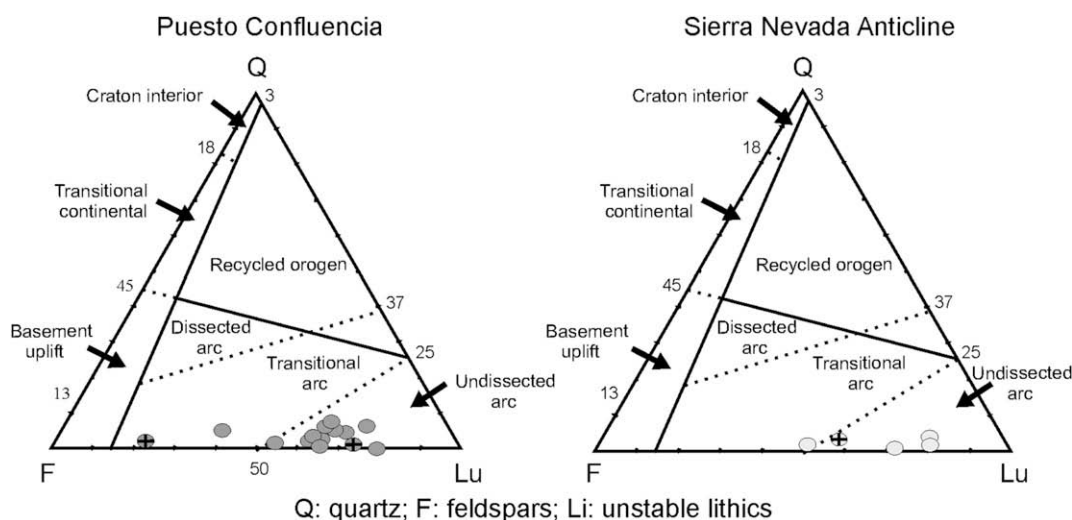

Fig. 8. Sandstone samples plotted in QFLu provenance diagrams (Dickinson et al., 1983). Lu includes all lithic fragments except polycrystalline quartz (chert was not recognized). Dark gray circles: PC samples; clear gray circles: SNA samples. Those circles with cross belong to the upper member.

Table 2
Composition of pyroclastic framework grains from the Bajo Barreal Formation at PC and SNA localities. Cund: undifferentiated crystal. Lund: undifferentiated lithic. Gs: glass shard. P1: pumice with flattened vesicles. P2: pumice with rounded to ellipsoidal vesicles. Vund: undifferentiated vitric component. Remaining abbreviators are similar to those of Table 1

Sample #	Phenocrysts (%)															
	Qms	Or	Pc	Pa	Pca	Pp	Pz	Pzc	Pza	Pn	Pzn	Pap	Papz	Pcp	Pcaz	Cund
Sna 8	2.4	–	0.8	0.8	–	–	–	–	–	0.8	–	–	–	–	–	4.40
Sna 11	0.68	1.38	2.41	0.34	–	–	–	–	–	0.34	–	–	–	–	–	–
Sna 13	2.12	1.77	3.55	1.06	2.13	–	0.71	–	–	0.35	–	–	–	–	–	–
Sna 16	2.33	1.46	1.46	1.75	0.58	–	–	–	–	0.88	–	–	–	–	–	–
Sna 17	4.09	4.09	1.36	1.36	0.34	–	0.34	–	–	1.71	–	–	–	–	–	–
Sna 18	4.8	4.17	0.96	5.45	1.60	0.64	2.56	0.32	1.28	0.64	0.64	0.32	–	–	–	–
Sna 19	2.32	5.31	2.32	2.66	0.66	–	–	–	–	1.66	–	–	–	–	0.66	–
Sna 30	4.41	5.51	0.37	0.37	3.31	–	–	–	–	0.73	–	–	–	0.37	–	–
Pc 6	1.13	2.26	1.51	1.51	1.13	–	0.38	–	–	0.75	–	–	–	–	–	8.68
Pc 22	1.09	1.82	1.09	1.09	0.73	–	–	–	–	0.73	–	–	–	–	–	2.91
Pc 25	0.68	–	–	–	–	–	–	–	–	1.37	–	–	–	–	–	1.03
Pc 41	1.55	3.1	1.16	3.1	0.77	0.39	1.55	0.77	–	–	–	–	0.39	–	–	1.94
Pc 45	2.54	5.09	2.18	2.91	–	–	–	–	–	0.36	–	–	–	–	–	–
Pc 50	1.70	0.68	1.02	0.68	0.34	–	–	–	–	0.34	–	–	–	–	–	3.75
Pc 59	1.46	–	0.73	–	–	–	1.83	–	0.37	–	–	–	–	–	–	2.20

Sample #	Lithoclasts (%)							Vitroclasts (%)			Accesory minerals (%)				Total
	Lvg	Lvp	Lvt	Lvpi	Lve	Lund	Gs	P1	P2	Vund	Amp	Mc	Op	Alt	
Sna 8	1.20	3.20	–	0.80	–	–	76.00	0.40	–	6.80	–	0.40	1.20	0.80	100
Sna 11	1.38	4.14	0.69	–	–	–	29.31	18.97	36.55	–	–	0.34	0.34	3.10	100
Sna 13	3.90	4.96	2.13	1.77	–	–	14.54	19.15	35.82	–	0.35	–	0.35	5.32	100
Sna 16	2.63	0.88	1.46	0.58	3.80	–	15.79	21.35	40.94	–	–	–	1.17	2.92	100
Sna 17	–	0.68	–	–	–	–	65.87	6.83	7.85	–	–	1.02	1.02	3.41	100
Sna 18	–	0.64	–	–	1.60	–	19.87	21.15	27.56	–	–	3.53	0.96	1.28	100
Sna 19	1.33	1.00	1.00	–	–	–	67.77	7.97	1.66	–	–	1.99	1.00	0.66	100
Sna 30	2.21	0.37	–	0.74	9.56	–	19.48	39.7	12.5	–	–	–	–	0.37	100
Pc 6	1.89	2.26	–	–	1.51	–	45.28	13.59	13.59	–	–	1.13	1.13	2.26	100
Pc 22	0.73	1.45	–	–	3.27	2.18	24.00	35.64	21.45	–	–	–	–	1.82	100
Pc 25	1.03	1.37	0.69	–	–	1.03	27.15	44.67	14.09	3.09	–	–	–	3.78	100
Pc 41	–	–	0.78	1.94	2.33	–	25.19	33.72	17.05	1.55	–	–	0.77	1.94	100
Pc 45	2.18	1.82	–	–	2.55	–	14.91	12.73	44.37	3.64	–	–	0.73	4	100
Pc 50	0.68	2.05	–	–	2.73	–	51.19	10.92	17.06	–	–	–	1.71	5.12	100
Pc 59	–	0.37	0.37	–	1.83	–	28.21	14.29	46.89	–	–	–	0.37	1.10	100

and hornblende. Clay coatings and microgranular quartz are ubiquitous cement types; sparry calcite and analcime patches occur in some samples. Clinoptilolite, generally filling dissolved pyroclastic grains, constitute an important cement type only in PC samples. Optical porosity ranges from 0% to 2.5% at SNA ($\overline{X} = 0.31\%$) and 0% to 6.5% at PC ($\overline{X} = 2.15\%$); and no hydrocarbon impregnation was observed at both localities. Using the ternary classification diagram of Schmid (1981), all samples are classified as vitric tuffs with a homogeneous composition near the V apex. The average compositions are $C_{11}V_{84}L_5$ and $C_{15}V_{80}L_5$ for the tuffs and tuffo-psammites of PC and SNA, respectively.

8. Geochemistry of sandstones and pyroclastic rocks

8.1. Major elements

Table 3 shows the major element composition (wt%) and CIA values for the Bajo Barreal Formation sandstones and tuffs/tuffo-
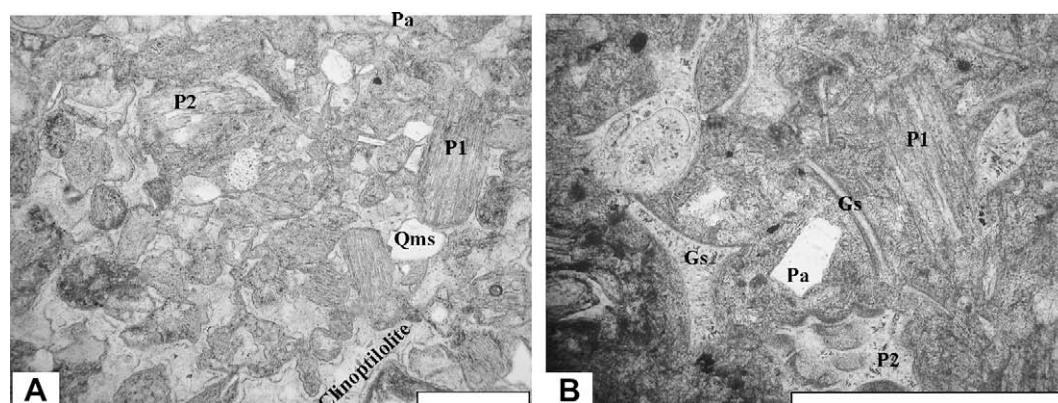
Fig. 9. Microphotographs of the Bajo Barreal Formation pyroclastic rocks. A, general view of pumice-rich vitric tuff (PC25) showing abundant pumice with flattened vesicles (P1) and minor amount of pumice with rounded vesicles (P2), monocristalline quartz with straight extinction (Qms) and plagioclase twined according to albite law (Pa); note the presence of zeolitic cement (clinoptilolite). B, general view of glass shard-rich tuff (PC6) showing cuspate or platy glass shards (Gs), pumice (P1 and P2) and albite twined plagioclase (Pa). Scale bars = 0.5 mm, parallel light.

Table 3
Major element concentrations (wt%) and CIA values of Bajo Barreal Formation sandstones and tuffs/tuffo-psammites. Average composition by locality are also estimated. The CIA was not calculated for samples # PC25, PC33, PC35, PC36, SNA14 and SNA18 because of high content of calcite cement

Sample #	SiO_2	TiO_2	Al_2O_3	Fe_2O_3(t)	MnO	MgO	CaO	Na_2O	K_2O	P_2O_5	LOI	Total	CIA
Sandstones													
Pc 5	66.42	0.574	16.24	4.71	0.319	0.61	2.79	5.01	1.69	0.04	2.38	100.8	51.74
Pc 7	72.26	0.27	14.05	0.85	0.015	0.24	1.87	5.3	1.95	0.03	3.06	99.9	49.68
Pc 8	68.98	0.258	16.75	1.23	0.028	0.17	2.07	6.65	1.4	0.03	3.14	100.7	50.80
Pc 9	73.04	0.291	11.94	2.45	0.047	0.52	1.18	3.03	3.44	0.03	3.71	99.68	52.38
Pc 15	63.53	0.536	15.53	3.59	0.077	0.56	2.95	4.21	2.08	0.06	6.34	99.46	51.64
Pc 16	68.55	0.419	11.88	2.88	0.096	0.59	2.02	3.17	1.71	0.04	7.85	99.21	52.52
Pc 19	64.57	0.54	16.52	4.63	0.157	0.48	3.07	4.56	2.21	0.06	2	98.81	51.63
Pc 20	65.87	0.636	13.77	6.71	0.234	0.67	2.23	3.46	2.69	0.2	4.18	100.7	52.10
Pc 28	72.35	0.284	13.38	1.05	0.021	0.12	2.4	4.1	1.97	0.05	4.37	100.1	50.26
Pc 29	65.24	0.329	14.67	2.68	0.075	0.32	2.38	4.5	2.09	0.04	7.42	99.74	51.18
Pc 31	62.66	0.592	15.73	5.35	0.16	0.54	2.87	4.41	2.07	0.08	6.52	101	51.67
Pc 33	48.67	0.792	12.96	3	0.857	0.3	14.47	3.92	1.4	0.06	12.51	98.94	–
Pc 35	68.12	0.291	13.15	2.21	0.088	0.62	3.01	3.62	1.67	0.07	7.73	100.6	–
Pc 36	60.92	0.491	14.13	2.55	0.254	0.46	5.4	3.92	1.9	0.14	8.82	98.97	–
Pc 40	66.03	0.307	15.23	2.03	0.056	0.49	3.31	4.44	1.54	0.05	7	100.5	50.39
Pc 43	72.56	0.34	13.4	1.88	0.032	0.21	1.69	4.69	1.52	0.02	2.68	99.02	51.87
Pc 51	65.11	0.815	15.6	3.1	0.094	0.55	2.6	4.53	2.82	0.12	4.67	100	50.59
Pc 52	60.03	0.738	16.99	4.23	0.216	0.74	4.16	5.38	1.52	0.12	6.6	100.7	48.47
Pc 57	62.71	0.587	15.73	3.68	0.076	0.78	3.42	4.2	1.41	0.11	8.1	100.8	51.77
Pc 63	72.02	0.536	12.34	1.56	0.036	0.23	2.44	3.46	1.41	0.07	5.86	99.97	51.42
Average	65.98	0.48	14.50	3.02	0.15	0.46	3.32	4.33	1.92	0.07	5.74	99.98	51.18
Sna 14	65.36	0.531	13.66	3.02	0.07	0.72	3.11	3.62	1.54	0.04	9.01	100.7	–
Sna 15	67.92	0.34	11.03	3.14	0.088	0.87	2.21	2.78	1.57	0.04	9.48	99.46	51.73
Sna 24	65.87	0.428	13.75	2.83	0.068	1.18	2.21	2.44	3.35	0.05	7.84	100	54.11
Sna 27	67.27	0.209	11.63	1.68	0.022	0.9	1.66	2.23	2.18	0.1	11.01	98.89	56.24
Sna 36	62.36	0.917	15.61	4.46	0.079	0.87	3.68	3.89	1.81	0.11	5.33	99.11	50.91
Average	65.75	0.48	13.14	3.03	0.06	0.91	2.57	2.99	2.09	0.07	8.53	99.63	53.24
Tuffs and tuffo-psammites													
Pc 6	78.32	0.288	8.58	2.7	0.047	0.72	0.59	1.61	3.3	0.02	3.56	99.73	54.05
Pc 22	65.47	0.428	12.94	3.16	0.067	0.73	2.18	2.3	1.06	0.03	10.6	98.95	59.26
Pc 25	66.79	0.356	11.83	2.8	0.06	0.46	1.7	3.33	1.64	0.03	10.51	99.5	–
Pc 41	59.55	0.551	15.06	5.52	0.079	1.45	3.02	2.91	1.41	0.05	10.75	100.4	56.06
Pc 45	73.52	0.273	12.7	1.4	0.04	0.16	0.69	5.42	1.74	0.03	4.03	100	51.30
Pc 50	67.47	0.263	12.31	2.05	0.069	0.89	1.73	2.08	2.85	<0.01	11.12	100.8	56.05
Pc 59	69.4	0.386	11.16	1.7	0.017	0.62	1.61	2.25	2.2	0.01	10.18	99.54	55.33
Average	68.64	0.36	12.08	2.76	0.05	0.72	1.64	2.84	2.03	0.02	8.68	99.84	55.34
Sna 7	74.67	0.402	9.44	2.7	0.076	1.02	1.62	1.53	2.88	0.06	6.25	100.6	52.38
Sna 11	66.94	0.292	11.29	2.48	0.053	0.61	2.13	3.14	1.7	0.03	10.85	99.51	50.92
Sna 13	67.16	0.3	10.77	2.47	0.11	0.67	2.37	3.7	1.52	0.03	10.43	99.52	47.21
Sna 16	68.88	0.373	11.72	2.4	0.069	0.69	2.09	2.53	2.69	0.04	8.5	99.99	51.87
Sna 17	70.97	0.228	11.1	2.46	0.037	0.78	1.73	2.44	2.62	<0.01	8.03	100.4	52.61
Sna 18	66.95	0.384	12.97	2.93	0.051	0.77	2.65	3.64	1.9	0.14	7.58	99.95	–
Sna 19	68.29	0.235	11.96	2.16	0.026	0.68	1.99	2.69	2.87	0.05	8.63	99.6	51.75
Sna 30	65.08	0.286	12.73	2.56	0.109	1.65	1.81	1.88	0.81	0.04	11.73	98.69	63.68
Average	68.46	0.30	11.51	2.3	0.06	0.86	2.03	2.64	2.13	0.05	9.22	99.68	52.92

psammites. In comparison with the Post-Archean Australian Shale (PAAS) standard, whose use have been advised for sedimentary rocks by Taylor and McLennan (1985), the average sandstone for each locality has very similar SiO_2 content and is enriched in CaO and Na_2O, whereas other oxides are depleted (Fig. 10). The mean MnO content from PC sandstones is greater than that of SNA and the PAAS, because of the occurrence of five samples with anomalously high concentration of MnO (samples # PC5, PC20, PC33, PC36 and PC52). CIA ranges from 48.47 to 52.52 ($\overline{X} = 51.18$) for PC sandstones and from 50.91 to 56.24 ($\overline{X} = 53.24$) for SNA sandstones. The sandstone samples of both localities were characterized using the Roser and Korsch's (1988) diagram (Fig. 11), which employ two discriminant functions that have been shown to accurately identify the provenance of sandstones (Ryan and Williams, 2007).

Tuffs and tuffo-psammites are mostly dacitic in composition as suggested by the samples plotted in the TAS diagram (total alkalis versus SiO_2; Le Maitre et al., 1989; Fig. 12). Only four samples show a different composition: one plots in the field of andesite (PC41); and three in the field of rhyolite (PC6, PC45 and SNA7). According to Richwood (1989), all samples belong to the subalkaline series and
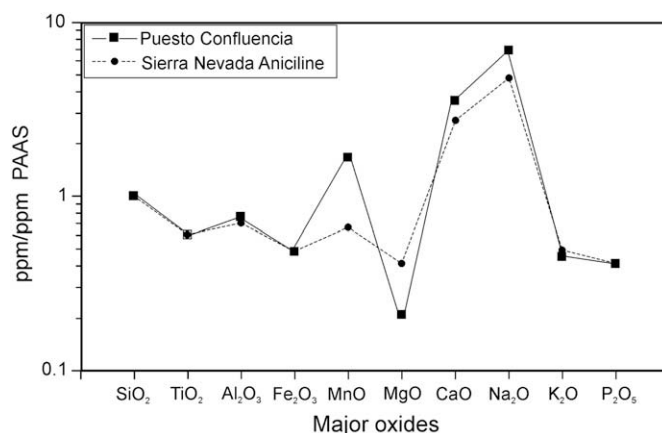

Fig. 10. Average composition of major oxides from the Bajo Barreal Formation sandstones normalized against PAAS (Taylor and McLennan, 1985).
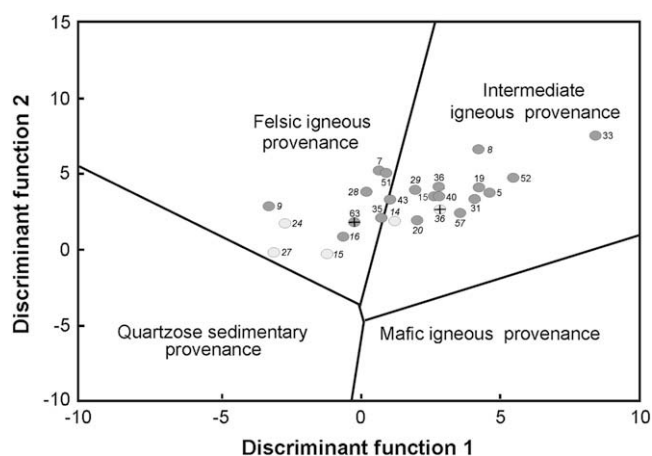
Fig. 11. Discriminant diagram for the Bajo Barreal Formation sandstone samples (Roser and Korsch, 1988). Discriminant function $1 = -1.773TiO_2 + 0.607Al_2O_3 + 0.76Fe_2O_3(t) - 1.5MgO + 0.616CaO + 0.509Na_2O - 1.224 K_2O - 9.09$. Discriminant function $2 = 0.445TiO_2 + 0.07Al_2O_3 - 0.25Fe_2O_3(t) - 1.142MgO + 0.438CaO + 1.475Na_2O + 1.426 K_2O - 6.861$. Dark gray circles: PC samples; clear gray circles: SNA samples. Those circles with cross belong to the upper member.

plot within the medium-K type field in the K_2O versus SiO_2 Harker's diagram of Le Maitre et al. (1989; Fig. 13). CIA is also low in both localities; this index ranges from 51.30 to 59.26 at PC ($\overline{X} = 55.34$) and for 47.21 to 63.68 at SNA ($\overline{X} = 52.92$).
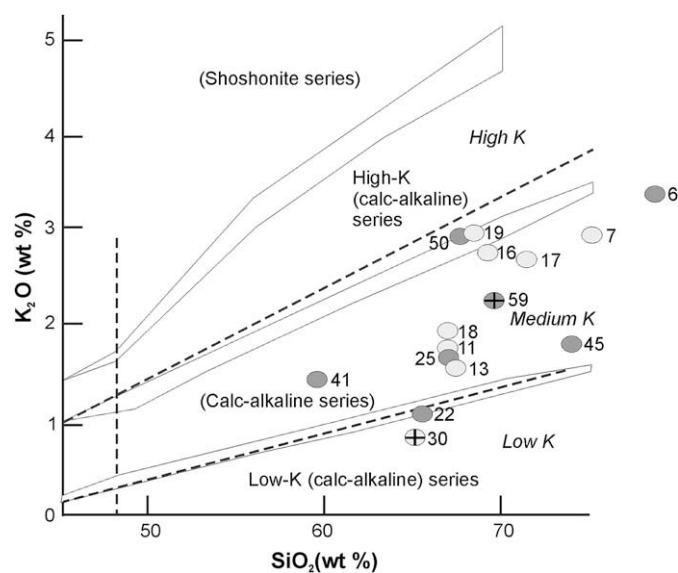

Fig. 13. Harker's diagram (K_2O versus SiO_2 wt%) for the tuffs and tuffo-psamites of the Bajo Barreal Formation. The samples from PC were plotted as dark gray circles and those from SNA were plotted as clear gray circles. The cross indicates that the sample belong to the upper member.
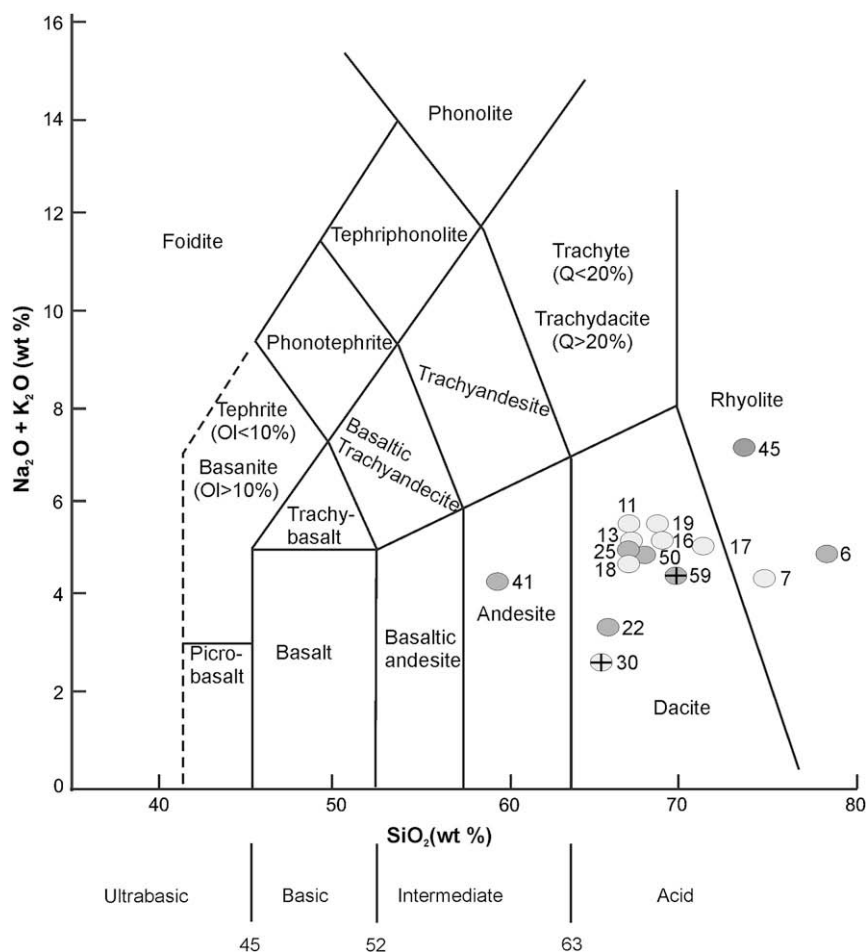

Fig. 12. TAS diagram (Le Maitre et al., 1989) for the tuffs and tuffo-psammites of the Bajo Barreal Formation. Dark gray circles: PC samples; clear gray circles: SNA samples. The cross indicates that the sample belong to the upper member.

Table 4
Trace element concentrations, including rare earth elements, for the sandstones and tuffs/tuffo-psammites of the Bajo Barreal Formation (in ppm)

Sample	Sc	Be	V	Cr	Co	Ni	Cu	Zn	Ga	Ge	As	Rb	Sr	Y	Zr
Sandstones															
Pc 5	9	1	78	20	7	<20	<10	60	20	1.5	6	59	343	19.2	144
Pc 7	5	<1	23	30	4	<20	<10	<30	11	1.1	<5	75	216	15.2	88
Pc 8	4	<1	22	<20	2	<20	<10	<30	12	1	<5	57	241	16.5	97
Pc 9	6	<1	30	<20	3	<20	<10	<30	11	1.1	<5	134	110	27.2	133
Pc 15	10	2	41	<20	4	<20	<10	50	19	1.2	6	79	381	24.1	191
Pc 16	8	2	30	<20	4	<20	<10	70	15	1.6	<5	95	314	30.9	191
Pc 19	9	1	58	<20	4	<20	<10	70	20	1.8	<5	64	413	20.8	149
Pc 20	12	1	85	30	7	<20	<10	80	20	2	11	92	241	37.3	178
Pc 28	5	1	19	<20	2	<20	<10	40	13	2.3	<5	65	314	20.8	118
Pc 29	8	1	24	<20	3	<20	<10	60	17	1.9	<5	85	314	36.6	175
Pc 31	12	1	44	<20	7	<20	<10	90	23	2.3	<5	77	327	32.1	239
Pc 33	8	2	40	<20	2	<20	<10	90	18	1	<5	40	306	18.5	137
Pc 35	5	<1	20	<20	3	<20	<10	40	14	0.9	5	84	300	17.3	141
Pc 36	10	1	30	<20	4	<20	<10	60	17	0.9	<5	70	357	28.8	120
Pc 40	6	1	30	40	2	<20	<10	40	15	0.8	<5	45	423	16.2	138
Pc 43	6	1	28	60	5	<20	<10	60	13	1	6	49	221	14.4	124
Pc 51	12	1	42	<20	3	<20	<10	90	17	1.4	<5	89	379	39.1	205
Pc 52	14	1	45	30	3	<20	<10	80	17	1.4	<5	38	543	21.4	171
Pc 57	12	2	37	<20	3	<20	<10	60	17	0.8	<5	43	462	34.4	239
Pc 63	8	<1	116	<20	2	<20	<10	50	11	0.6	<5	51	451	18.1	144
Average	8.45	1.27	42.1	35	3.7	–	–	64.11	16	1.33	6.8	69.55	332.8	24.44	156.1
Sna 14	12	2	44	<20	4	<20	<10	50	14	1.1	<5	62	342	25.9	161
Sna 15	9	1	38	<20	4	<20	<10	40	12	1.6	<5	84	234	22.9	145
Sna 24	9	2	49	<20	3	<20	20	50	16	1.4	<5	107	264	27.8	165
Sna 27	7	2	8	<20	1	<20	<10	50	15	0.9	<5	75	443	39.8	162
Sna 36	16	1	55	<20	4	<20	<10	90	18	1.1	<5	53	508	23.8	249
Average	10.6	1.6	38.8	–	3.2	–	20	56	15	1.22	–	76.2	358.2	28.04	176.4
Tuffs and tuffo-psammites															
Pc 6	6	1	22	<20	2	<20	10	50	17	1.5	<5	125	50	25.3	109
Pc 22	10	1	30	<20	3	<20	20	40	16	2	<5	55	144	29	143
Pc 25	10	1	20	<20	3	<20	<10	70	16	4.3	<5	90	135	34.3	206
Pc 41	13	2	44	<20	5	<20	<10	70	21	1.2	<5	60	276	30	186
Pc 45	10	<1	22	<20	4	<20	<10	50	9	1	7	68	87	25.6	182
Pc 50	7	1	12	<20	2	<20	<10	40	13	0.7	<5	67	168	28.9	174
Pc 59	11	1	22	<20	2	<20	<10	50	11	<0.5	<5	70	263	24.1	150
Average	9.57	1.17	24.57	–	3	–	15	52.86	14,71	1.78	7	76.43	160.43	28.17	164.28
Sna 7	10	<1	98	<20	3	<20	<10	40	12	1.9	<5	90	133	28.4	135
Sna 11	8	2	25	<20	3	<20	<10	50	13	1.1	<5	85	226	28.8	157
Sna 13	8	2	27	<20	3	<20	<10	40	12	1.5	<5	68	204	25.7	149
Sna 16	9	1	58	<20	3	<20	<10	50	12	1.8	7	93	249	24.1	150
Sna 17	5	1	32	<20	3	<20	<10	30	11	1.3	<5	115	254	14.3	113
Sna 18	6	2	44	20	2	<20	<10	60	16	1.4	<5	109	305	19.7	166
Sna 19	8	2	39	<20	2	<20	<10	40	12	1.6	<5	135	348	20.2	127
Sna 30	6	<1	21	<20	2	<20	<10	40	13	1.7	<5	36	235	38.3	121
Average	7.44	1.71	39.11	20	2.44	–	–	44.44	12.89	1.47	7	89.55	266.33	26.59	142.22

Sample	Nb	Mo	Ag	In	Sn	Sb	Cs	Ba	La	Ce	Pr	Nd	Sm	Eu	Gd
Sandstones															
Pc 5	5	3	<0.5	<0.1	<1	1.6	4.2	667	20.1	40.1	4.62	16.5	3.73	1.59	3.08
Pc 7	2.9	3	<0.5	<0.1	<1	1.4	15	466	13.4	26.4	3.26	11.5	2.62	0.98	2.19
Pc 8	3.4	<2	<0.5	<0.1	<1	1.5	20.9	469	15.1	30	3.67	13.4	3.02	1.07	2.53
Pc 9	5.1	2	<0.5	<0.1	<1	1.2	10.9	467	24.7	49.8	6.3	22.2	5.02	1.01	4.13
Pc 15	6.7	4	<0.5	<0.1	1	0.9	4.1	1304	25.9	50.8	5.91	22.9	4.81	1.75	4.29
Pc 16	7.8	<2	<0.5	<0.1	2	2	3.2	1506	28.2	58.1	6.79	25.8	5.6	1.21	5.13
Pc 19	4.8	<2	<0.5	<0.1	<1	2.4	1.2	655	22.2	40.2	4.92	18.7	3.88	1.99	3.65
Pc 20	6.7	6	<0.5	<0.1	2	5	2.2	659	30.1	56.9	7.52	30.1	6.89	1.72	6.54
Pc 28	4.1	<2	<0.5	<0.1	<1	1.4	2	807	19.8	40.5	4.57	17.4	3.82	1.77	3.37
Pc 29	6.5	<2	<0.5	<0.1	2	1.5	2.8	1079	31.1	62.5	7.47	28.7	6.25	1.66	5.58
Pc 31	7.9	<2	<0.5	<0.1	1	1.6	2.8	932	22.1	43.8	5.42	21.8	5.02	1.86	4.96
Pc 33	7.9	<2	<0.5	<0.1	1	2	1	564	14.1	26.8	3.35	12.4	2.52	1.39	2.36
Pc 35	5.2	85	<0.5	<0.1	1	1.3	3.8	840	17.2	34	3.75	13.9	2.83	0.872	2.7
Pc 36	4.5	36	<0.5	<0.1	1	1.4	2.7	732	18.6	39.2	4.72	19	4.35	1.49	4.46
Pc 40	4.6	<2	<0.5	<0.1	<1	2.3	2.2	699	16.8	34	3.94	15.5	3.45	1.44	3.17
Pc 43	3.8	<2	<0.5	<0.1	<1	1.2	12.4	501	15	29.9	3.44	13.2	2.96	1.2	2.58
Pc 51	7.8	<2	<0.5	<0.1	1	1.9	2.8	701	23.1	48.1	5.95	24.5	5.9	2	5.9
Pc 52	5.5	<2	<0.5	<0.1	1	1.7	1.4	690	17.8	37.4	4.56	18.7	4.33	2.24	4.04
Pc 57	7.2	2	<0.5	<0.1	1	1.9	1.9	674	24.3	50.5	6.44	26.8	5.94	1.91	5.83
Pc 63	6	<2	<0.5	<0.1	<1	2.7	2.2	773	16.8	34.3	4.07	15.7	3.43	1.22	3.17
Average	5.67	17.62	–	–	1.27	1.84	4.98	759.25	20.82	41.66	5.03	19.43	4.32	1.52	3.98
Sna 14	6.3	<2	<0.5	<0.1	1	1.5	4.8	634	19.4	43.4	5.12	19.9	4.59	1.31	4.48
Sna 15	5.6	<2	<0.5	<0.1	1	1.2	5.6	536	21.3	46	5.29	20.7	4.59	1.03	4.3
Sna 24	7.6	<2	<0.5	<0.1	2	1.9	3.7	516	25.2	49.8	5.96	21.5	4.15	1.1	3.98
Sna 27	8	<2	<0.5	<0.1	2	1.9	1.7	953	28.8	58.7	7.36	28.3	5.87	1.17	6.1
Sna 36	8.2	<2	0.6	<0.1	1	1.3	1.4	849	18.4	38.1	4.59	18.8	4.23	1.71	4.22

Table 4 (*continued*)

Sample	Nb	Mo	Ag	In	Sn	Sb	Cs	Ba	La	Ce	Pr	Nd	Sm	Eu	Gd
Average	7.14	–	0.6	–	1.4	1.56	3.44	697.6	22.62	47.2	5.66	21.84	4.69	1.26	4.62
Tuffs and tuffo-psammites															
Pc 6	5.7	5	<0.5	<0.1	2	2.5	6.6	376	14	29.3	3.66	13.7	3	0.84	3.22
Pc 22	6.6	<2	<0.5	<0.1	2	1.4	4.8	473	23.6	52.5	6.02	23.6	5.29	1.12	4.78
Pc 25	8	<2	<0.5	<0.1	2	1.6	7.8	606	28.8	60.7	7.23	27.9	6.29	1.16	5.88
Pc 41	6.5	<2	<0.5	<0.1	2	1.3	3.2	602	22.4	47.5	5.78	23.5	5.74	1.45	5.53
Pc 45	5.8	8	0.5	<0.1	1	1.5	23.2	405	25.4	56.8	5.94	21.6	4.5	0.88	4.07
Pc 50	6.2	<2	<0.5	<0.1	1	1.2	1.3	339	22.6	49.6	5.96	24	5.4	1.21	4.86
Pc 59	4.7	<2	<0.5	<0.1	1	1.2	3.7	519	21.6	44.6	5.64	22	4.94	1.1	4.7
Average	6.21	6.5	0.5	–	1.57	1.53	7.23	474.28	22.63	48.71	5.75	22.33	5.02	1.11	4.72
Sna 7	4.8	<2	<0.5	<0.1	1	1.4	3.2	364	18.9	41.5	5.2	20.6	4.89	1.05	4.64
Sna 11	6.8	<2	<0.5	<0.1	2	1.4	6.8	657	25.5	53.8	6.31	24.7	5.43	1.05	5.2
Sna 13	6.1	<2	<0.5	<0.1	1	1.3	5.8	520	21.4	46.1	5.32	21.2	4.61	0.95	4.4
Sna 16	5.7	<2	<0.5	<0.1	1	1.6	4.9	568	18.9	42.9	5.04	19.6	4.37	1.12	4.08
Sna 17	5.3	<2	<0.5	<0.1	1	1.4	4.9	663	19.5	39.8	4.09	14.4	2.82	0.53	2.48
Sna 18	7.1	<2	<0.5	<0.1	1	3.4	6.4	626	30	55.7	6.04	20.9	3.47	0.84	3.06
Sna 19	5.9	<2	<0.5	<0.1	1	1.3	3.4	945	23.8	47.9	5.4	19.8	4.08	0.79	3.8
Sna 30	5	<2	<0.5	<0.1	1	1.3	2.6	748	25.6	49.4	5.61	20.9	4.39	0.85	4.56
Average	6.08	–	–	–	1.22	1.67	4.41	671.55	23.6	48.42	5.60	21.15	4.44	0.93	4.26

Sample	Tb	Dy	Ho	Er	Tm	Yb	Lu	Hf	Ta	W	Tl	Pb	Bi	Th	U
Sandstones															
Pc 5	0.53	3.06	0.63	1.97	0.31	2.01	0.30	3.8	0.25	0.7	1	24	0.3	5.87	1.6
Pc 7	0.37	2.23	0.48	1.65	0.26	1.7	0.26	2.2	0.17	0.6	0.45	24	0.4	5.25	1.13
Pc 8	0.43	2.51	0.52	1.67	0.25	1.68	0.26	2.4	0.18	<0.5	0.48	36	0.5	5.09	2.32
Pc 9	0.69	4.08	0.85	2.8	0.43	2.81	0.42	3.6	0.32	0.7	0.67	19	0.8	9.8	2.21
Pc 15	0.68	3.95	0.79	2.4	0.38	2.58	0.39	4.7	0.47	1	0.62	18	<0.1	7.37	1.84
Pc 16	0.83	4.89	0.99	3.09	0.5	3.34	0.50	5.6	0.64	1.1	0.69	33	0.8	10.3	2.34
Pc 19	0.59	3.46	0.72	2.18	0.35	2.35	0.34	3.7	0.36	1.2	0.68	22	0.2	5.13	1.69
Pc 20	1.02	5.95	1.17	3.63	0.55	3.61	0.55	4.6	0.54	1.8	1.06	47	0.5	7.64	2.52
Pc 28	0.55	3.16	0.66	2.02	0.31	2.15	0.32	2.7	0.32	<0.5	0.54	30	0.8	6.22	1.76
Pc 29	0.92	5.53	1.14	3.6	0.55	3.59	0.54	4.5	0.52	1	0.56	38	0.7	9.03	2.19
Pc 31	0.82	5.11	1.11	3.56	0.58	3.99	0.63	6.3	0.51	1	0.57	26	0.6	7.17	1.93
Pc 33	0.42	2.56	0.55	1.95	0.31	2.09	0.32	3.6	0.32	1	0.36	57	1.1	3.44	5.1
Pc 35	0.43	2.5	0.52	1.66	0.27	1.8	0.28	3.3	0.41	<0.5	1.26	17	0.4	6.86	2.07
Pc 36	0.74	4.41	0.91	2.7	0.40	2.52	0.38	3.1	0.3	<0.5	0.82	23	0.6	5.18	1.54
Pc 40	0.51	2.86	0.55	1.64	0.25	1.73	0.25	3.3	0.33	<0.5	0.34	23	0.4	5.57	0.96
Pc 43	0.39	2.31	0.47	1.49	0.24	1.66	0.23	3	0.27	0.6	0.41	30	<0.1	4.54	2.88
Pc 51	0.99	6.05	1.25	3.87	0.60	4.05	0.62	5	0.51	0.8	0.7	37	0.8	6.99	2.14
Pc 52	0.68	3.85	0.79	2.36	0.38	2.61	0.39	4.2	0.4	0.6	0.43	35	0.4	5.52	2.07
Pc 57	0.94	5.46	1.12	3.5	0.54	3.57	0.53	5.7	0.52	<0.5	0.2	26	0.4	6.7	1.95
Pc 63	0.51	2.97	0.59	1.85	0.29	1.95	0.30	3.6	0.42	1.1	0.25	20	0.3	5.8	1.27
Average	0.65	3.84	0.79	2.48	0.39	2.59	0.40	3.94	0.39	0.94	0.60	29.25	0.56	6.47	2.07
Sna 14	0.75	4.4	0.88	2.74	0.43	2.83	0.42	4.1	0.47	<0.5	0.52	31	0.8	7.3	2.3
Sna 15	0.69	3.89	0.78	2.43	0.38	2.49	0.37	3.7	0.46	1.4	0.42	23	0.5	7.73	1.94
Sna 24	0.73	4.49	0.94	3.04	0.48	3.18	0.48	4.5	0.51	0.8	1.13	86	2.7	8.57	2.41
Sna 27	1.06	6.13	1.22	3.75	0.56	3.46	0.48	4.9	0.52	<0.5	0.44	117	2.7	9.97	2.23
Sna 36	0.68	3.98	0.81	2.54	0.39	2.74	0.42	5.4	0.66	<0.5	0.36	25	0.6	5.34	1.28
Average	0.78	4.58	0.93	2.9	0.45	2.94	0.44	4.52	0.52	1.1	0.57	56.4	1.46	7.78	2.03
Tuffs and tuffo-psammites															
Pc 6	0.63	4.01	0.82	2.65	0.42	2.72	0.40	3.6	0.48	1	1.02	92	5.2	9.14	5.65
Pc 22	0.81	4.9	0.97	2.98	0.48	3.18	0.47	3.9	0.55	1.6	0.41	26	0.8	9.25	1.81
Pc 25	0.95	5.59	1.14	3.45	0.57	3.78	0.56	5.4	0.67	<0.5	0.5	43	0.7	9.56	1.89
Pc 41	0.88	4.91	0.99	2.99	0.45	3.02	0.46	5.2	0.49	<0.5	0.31	30	0.9	7.17	1.63
Pc 45	0.7	4.06	0.83	2.65	0.45	3.07	0.48	4.6	0.57	0.7	0.61	53	1.3	12.9	3.08
Pc 50	0.81	4.91	1.05	3.36	0.56	3.89	0.60	4.9	0.58	<0.5	0.5	17	0.6	10.8	2.23
Pc 59	0.77	4.3	0.86	2.63	0.41	2.73	0.41	3.6	0.41	1.3	0.34	28	0.6	6.82	2.03
Average	0.79	4.67	0.95	2.96	0.48	3.20	0.49	4.46	0.53	1.15	0.53	41.28	1.44	9.38	2.62
Sna 7	0.81	4.79	0.98	3.08	0.49	3.27	0.50	3.4	0.36	1.7	0.79	20	0.9	5.72	1.53
Sna 11	0.83	4.78	0.97	2.93	0.45	3.02	0.46	4.2	0.74	<0.5	0.59	50	0.9	9.05	2.49
Sna 13	0.73	4.21	0.85	2.57	0.41	2.72	0.41	3.9	0.55	<0.5	0.48	24	0.7	8.08	2.31
Sna 16	0.69	4.02	0.82	2.5	0.39	2.68	0.40	3.9	0.46	<0.5	0.81	36	0.8	8.2	2.16
Sna 17	0.41	2.39	0.48	1.5	0.26	1.82	0.28	3	0.57	<0.5	0.87	34	0.8	10.2	2.65
Sna 18	0.53	2.88	0.58	1.86	0.29	1.88	0.26	4.6	0.49	0.5	0.72	95	2.1	10.7	2
Sna 19	0.6	3.46	0.68	2.15	0.34	2.42	0.37	3.4	0.58	0.6	0.74	37	0.9	10.4	2.62
Sna 30	0.78	4.89	1.09	3.91	0.71	5.12	0.81	3.2	0.58	3.4	0.27	33	0.9	11.5	1.58
Average	0.71	4.17	0.85	2.69	0.44	2.93	0.45	3.83	0.54	1.55	0.63	49.55	1.17	9.31	2.17

8.2. Trace elements

Table 4 lists the trace element concentrations (ppm), including the rare earth elements (REE), for sandstones and tuffs/tuffo-psammites from the Bajo Barreal Formation. Chondrite normalized REE patterns (Taylor and McLennan, 1985) for the sandstones from PC and SNA localities are plotted in Fig. 14. REE patterns for both localities show moderate enrichment of LREE relative to HREE, the latter having a relatively flat pattern. The more remarkable difference between PC and SNA localities is the presence of a common
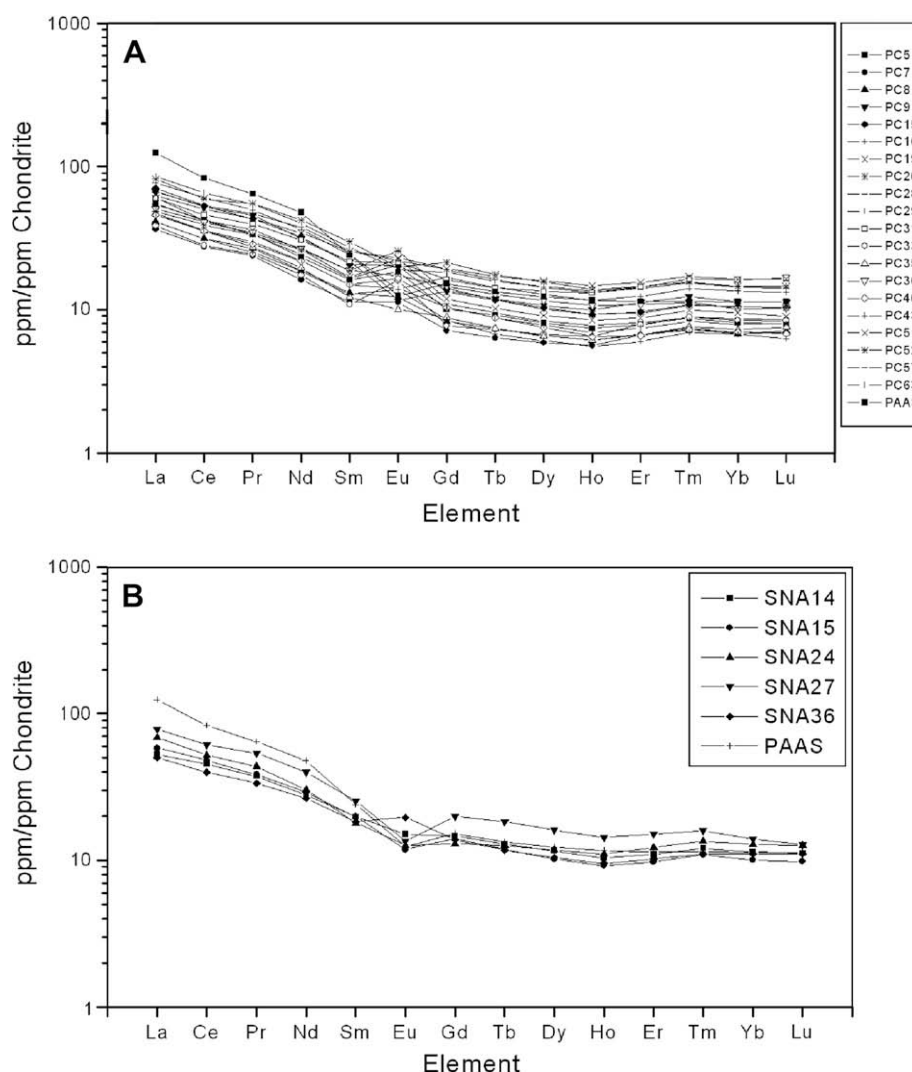
Fig. 14. Chondrite normalized REE patterns (Taylor and McLennan, 1985) of sandstone samples from the Bajo Barreal Formation: A, PC samples. B, SNA samples.

positive europium anomaly in the former. Petrographically, this difference is correlated with a major proportion of plagioclase and minor amount of pumice at PC (see Table 1). The range of Eu/Eu* is 0.59–1.22 ($\overline{X} = 0.84$) and 0.66–1.72 ($\overline{X} = 1.16$) for the northern and southern locality, respectively. Other elemental ratios, including La/ Sc, Th/Sc, Cr/Th and (La/Lu)$_N$, also can provide information about the provenance of sedimentary rocks (Table 5). La/Sc ratio has a minimum value of 1.76 and 1.15 for PC and SNA, respectively; reaching a maximum value of 4.11 in both localities. Th/Sc ratio ranges from 0.39 to 1.63 at PC and from 0.33 to 1.42 at SNA. Cr/Th ratio was not calculated for SNA samples because Cr concentrations are below of the detection limit; this ratio varies from 3.4 to 13.21 at PC. The range of (La/Lu)$_N$ ratio is 3.64–6.97 and 4.54–6.22 for PC and SNA, respectively.

Using the Zr/Ti versus Nb/Y classification diagram (Winchester and Floyd, 1977; modified by Pearce, 1996), the tuffs and tuffo-psammites are mostly classified as andesites + basaltic andesites (Fig. 15); only two samples from PC plot in the rhyolite + dacite field (samples # PC45 and PC50). A multi-element diagram normalized to Mid Ocean Ridge Basalt (MORB, Taylor and McLennan, 1985) using the average values for each locality is presented in Fig. 16. The most mobile elements are located on the left organized in order of increasing incompatibility; the remaining elements are considered
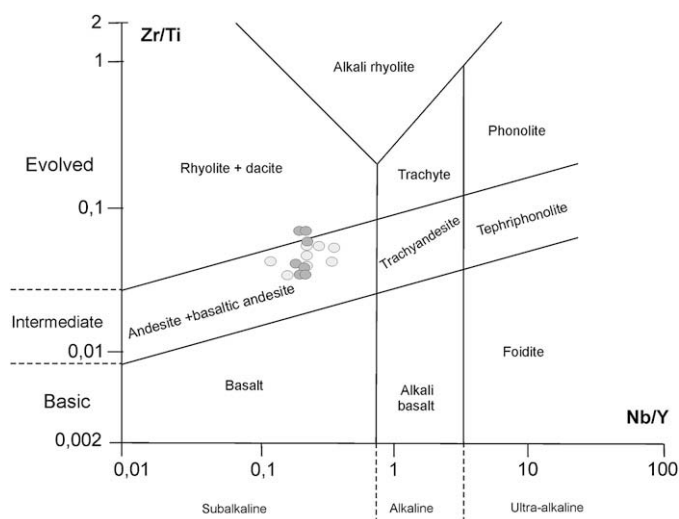
Fig. 15. Classification of the tuff and tuffo-psamite samples of the Bajo Barreal Formation using the Zr/Ti versus Nb/Y diagram (after Pearce, 1996). Dark gray circles: PC samples; clear gray circles: SNA samples. The cross indicates that the sample belong to the upper member.

immobile and are arranged in order of increasing incompatibility from right to left (cf. Ryan and Williams, 2007). The two profiles have parallel trends with enrichment in the low ionic potential elements, mainly in Rb and Th, and the profiles decreasing to right with a major depletion in the Ti and Sc elements.

In relation to sandstone samples, the pyroclastic samples of both localities exhibit similar chondrite-normalized (Taylor and McLennan, 1985) REE patterns, with a steeper La-Sm profile in comparison with a relatively flat pattern of HREE's elements (Fig. 17). All samples of pyroclastic rocks have Eu/Eu* values less than 1 (0.68 ± 0.25 for the southern locality and 0.64 ± 0.21 for the northern locality).

9. Discussion

9.1. Sandstone source-rocks

The sandstone samples with abundant volcanic lithic fragments, as well as the high content of plagioclase in relation to alkali feldspars and presence of inclusion-free quartz grains with straight extinction, suggest a source-rock lithology dominated by volcanic rocks (Folk, 1974; Dickinson and Suczek, 1979; Boggs, 1992). Oscillatory zonation in plagioclase is also a good indicator of a volcanic source (Pittman, 1969). The porphyritic and felsitic textures of the volcanic lithic fragments are commonly associated with a felsic effusive source, whereas the pilotaxitic and trachytic textures suggest an intermediate volcanic source-rock (Dickinson, 1970; Scasso and Limarino, 1997). The relative abundance of volcanic fragments with eutaxitic texture and pumice indicates a relatively important participation of pyroclastic volcanic rocks at the source area. Considering the four petrofacies recognized, PC samples exhibit a heterogeneous provenance from a felsic (petrofacies V1) to intermediate (petrofacies V2 and V4) volcanic source-rocks with abundant participation of a pyroclastic-rich source-rock lithology (petrofacies V3). SNA samples show a homogeneous provenance from pyroclastic-rich volcanic rocks (petrofacies V3).

The discrimination diagram of Roser and Korsch (1988) corroborates a provenance from felsic to intermediate igneous rocks for the channel sandstones (Fig. 11). In addition, values of selected trace element ratios including La/Sc, Th/Sc, Cr/Th, Eu/Eu* and (La/Lu)$_N$ (Table 5) for sandstones are more similar to those of sediments derived from felsic source rocks than those of mafic source rocks (e.g. Amstrong-Altrin et al., 2004). The low CIA values of sandstone samples (Table 3) indicate that the source region of these sediments experienced a low degree of weathering, resulting in slight removal of CaO and Na$_2$O. This interpretation is in agreement with the high content of plagioclase (as monocrystalline grains, phenocrysts and groundmass in lithic grains) determined by microscopic observations.

Table 5
Range of elemental ratios for the Bajo Barreal Formation sandstones compared with sandstones derived from felsic and mafic rocks (data from Amstrong-Altrin et al., 2004)

Elemental ratio	Range of Bajo Barreal sandstones		Range of sediments from felsic sources	Range of sediments from mafic sources
	PC	SNA		
La/Sc	1.76–4.11	1.15–4.11	2.50–16.30	0.43–0.86
Th/Sc	0.39–1.63	0.33–1.42	0.84–20.50	0.05–0.22
Cr/Th	3.40–13.21	–	4.00–15.00	25.00–500
Eu/Eu*	0.66–1.72	0.59–1.22	0.40–0.94	0.71–0.95
(La/Lu)$_N$	3.64–6.97	4.54–6.22	3.00–27.00	1.10–7.00

In addition to petrographic and geochemical data indicating a felsic to intermediate arc-related volcanic origin, the palaeocurrent data from cross-bedded channel sandstones in several localities of the western sector of the basin indicate palaeoflow directions from the west and northwest (Hechem, 1994, 1998; Bridge et al., 2000; Umazano et al., 2008). Considering the inferred source rock composition and tectonic setting; and palaeotransport directions toward the east and southeast, we suggest that the more possible source area is located to the west (cf. Tunik et al., 2004), where there are outcrops of Late Jurassic-Late Cretaceous volcanic successions belonging to the Patagonian Andes. The REE patterns of the Bajo Barreal Formation sandstones (using the average for each locality) and the roughly coeval Divisadero Formation volcanic rocks (values from Parada et al., 2001) are strikingly similar (Fig. 18), suggesting a possible derivation of the epiclastic rocks. This assumption is based on the relative immobility of the REE during weathering and transport (Ronov et al., 1974; Bathia, 1985); although a minor modification of the REE patterns due to burial diagenesis can not bee rash (McLennan et al., 2003). The positive europium anomaly recorded in the sedimentary rocks at PC can be attributed to a greater amount of plagioclase in the fluvial channel facies at this locality. A positive Eu anomaly in sedimentary rocks can be due to sedimentary sorting and does not necessarily reflect a source-inherited feature; in consequence this feature should not be used for provenance characterization (Taylor and McLennan, 1985; McLennan et al., 1993). A similar REE pattern between the Bajo Barreal and Ñirehuao formations, also suggest a possible contribution from this volcanic unit (Fig. 18). However, this contribution could be considered subordinate because Ñirehuao Formation displays larger participation of basaltic rocks and this mafic contribution is not reflected in neither detrital modes nor the geochemical data of the Bajo Barreal Formation sandstones.

9.2. Type of volcanism and location of volcanic edifices

Common dominance of pumice fragments with flattened or rounded to ellipsoidal vesicles in tuffs and tuffo-psammites suggests that plinian-like, highly explosive eruptions of viscous and volatile-rich magma were frequent (e.g. Mazzoni, 1986). Subordinately, tuff samples with a large amount of glass shards and common presence of R-type accretionary lapilli (Umazano et al., 2008) indicate subordinate phreatomagmatic-like explosive eruptions (Gilbert and Lane, 1994; Fisher and Schmincke, 1994). Deposition of pyroclastic sediments as ash-falls were commonly
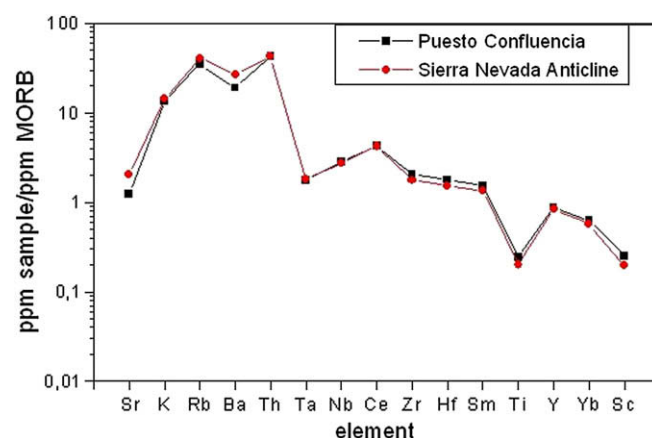

Fig. 16. Multi-element variation diagrams for the average tuff and tuffo-psamite samples of the Bajo Barreal Formation. Diagrams were plotted using MORB normalised data (Taylor and McLennan, 1985). A, PC. B, SNA.
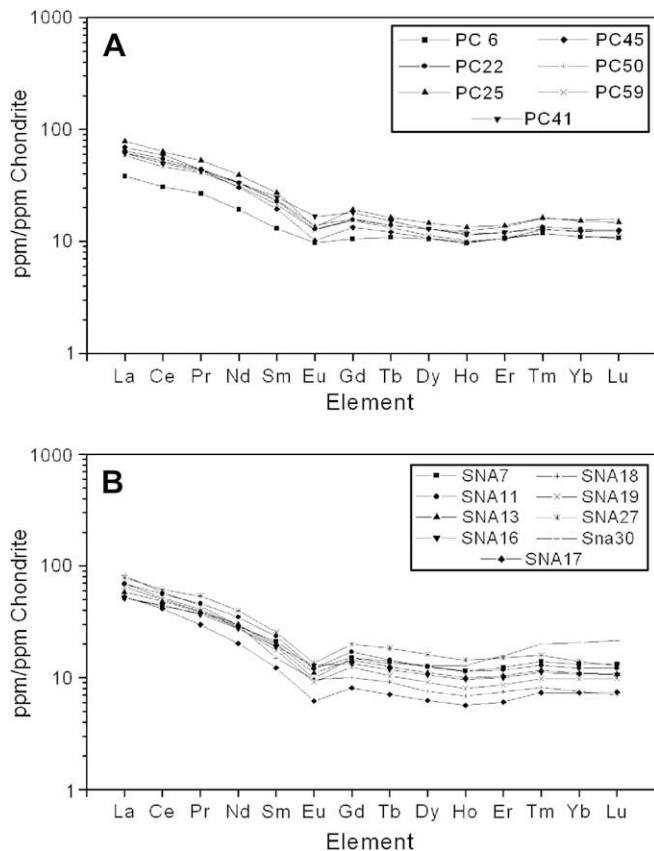
Fig. 17. Chondrite normalized REE patterns (Taylor and McLennan, 1985) of tuff-tuffo psamite samples from the Bajo Barreal Formation. A, PC. B, SNA.
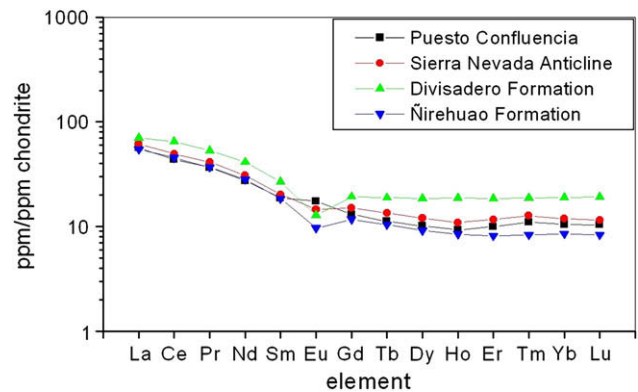

Fig. 18. Comparison between average REE pattern of the Bajo Barreal Formation sandstones by locality (this study) and the Divisadero and Ñirehuao formations volcanic rocks (Parada et al., 2001).

reworked by sheet-floods in floodplain environments (Umazano et al., 2008) and experienced a low degree of chemical weathering as suggested by CIA values (Table 3). This fact is probably a consequence of a rapid burial, in accordance with the weak development degree of associated andic palaeosols (Bellosi et al., 2002; Umazano et al., 2008). Higher values of CIA for tuffs and tuffo-psammites in comparison with those of associated channel sandstones can be related to a greater surface area and chemical instability of pyroclastic materials (mostly volcanic glass, pumice and vitric-vitrophyric fragments). Although the SiO_2 content is typical of felsic rocks, the Zr/Ti versus Nb/Y classification diagram (Pearce, 1996; Fig. 15) shows that the pyroclastic samples from the Bajo Barreal Formation are mostly compatible with derivation from intermediate magmatic precursors. It is considered that this interpretation is more likely because this diagram is based on the immobile trace element ratios. Negative europium anomaly observed in the Fig. 17 and Eu/Eu* < 1 values reflecting that Eu^{2+} was retained in the plagioclase within the magmatic sources and therefore the extracted melt resulted depleted in Eu (Winter, 2001; Best and Christiansen, 2001).

The MORB normalized profiles of the Fig. 16 are very similar to the pattern described by Pearce (1983) for active margin settings. Although the peak at Ce is also observed in island arc settings, the rock samples from this tectonic setting show a profile from Ta to Yb which is nearly flat and parallel to MORB values, which is not the case with the analyzed samples. Therefore, the high pyroclastic input arrived to the San Jorge Basin during sedimentation of the Bajo Barreal Formation were originated at an active continental margin. Moreover, the wide scatter of the positive linear trend in K_2O versus SiO_2 diagram (Fig. 13) may be attributable to the effects

of crustal contamination, typical of active continental margins (Wilson, 1989). Considering the presence of subduction processes at the western margin of Patagonia during deposition of the Chubut Group (Franzese et al., 2003; Folguera and Iannizzotto, 2004) and the geochemical affinity with the arc-related volcanic rocks, it is probable that the tuffs and tuffo-psammites of the Bajo Barreal Formation represent the distal eruptive counterpart of the Patagonian Bathotith. Based on the present separation between the studied localities and Patagonian Batholith outcrops, it is assumed that the eruptive centres were located at approximately 120 km to the west. The magnitude of the separation between vents and studied outcrops is consistent with a plinian-like volcanism (Heiken and Wohletz, 1992). Moreover, the dominance of channelled and sheet-flood fluvial processes (Umazano et al., 2008) suggest that Bajo Barreal Formation represent downstream equivalents of volcano-flanking fan or apron facies (Smith, 1988, 1991).

10. Conclusions

The composition and provenance of the Bajo Barreal Formation fluvial rocks at two selected localities (SNA and PC) in the western sector of the San Jorge Basin have been assessed using integrated petrographical, petrofacial and geochemical studies. These studies were focused on channel sandstones and associated pyroclastic floodplain deposits. The main conclusions of this work are:

(1) The channel sandstones are dominantly litharenites and feldspathic litharenites with abundant participation of volcanic lithic fragments showing different textures (porphyritic, eutaxitic, felsitic, pilotaxitic, trachytic and vitric-vitrophyric), pumice and plagioclase. K-feldspar, quartz and sedimentary rock fragments are scarce. Recognised cements include clay, quartz, analcime, clinoptilolite and calcite.
(2) QFLu diagram indicates a provenance from undissected-transitional arc. Several provenance indicators (type of rock fragments, K-feldspar/plagioclase ratio and inclusion-free quartz grains with straight extinction) suggest that the source rock lithology was constituted by felsic to intermediate volcanic rocks.
(3) Four sandstone petrofacies (V1 to V4) were defined for fluvial channel sandstones using cluster analysis considering the absolute abundance of the different volcanic lithic fragments and pumice. SNA sandstone samples belong only to petrofacies V3, indicating a pyroclastic-rich source rock lithology. In contrast, every petrofacies was recorded at PC denoting a more heterogeneous provenance from a felsic (petrofacies V1) to

intermediate (petrofacies V2 and V4) volcanic source-rocks with abundant participation of pyroclastic-rich layers (petrofacies V3).

(4) The floodplain tuffs and tuffo-psammites are glass-rich, essentially dominated by pumice fragments with rounded or ellipsoidal vesicles and, in few cases, by cuspate or platy glass shards. Phenocrysts (quartz, plagioclase and K-feldspar) and lithoclasts (volcanic lithic fragments) are subordinated components. The pyroclastic rocks show petrographical features mostly attributable to plinian-like explosive eruptions and, subordinately, to phreatomagmatic eruptions.

(5) Major oxides and trace element data confirm that the channel sandstones derive from a felsic to intermediate volcanic source rock, which experienced a low degree of chemical weathering. On the other hand, the floodplain pyroclastic rocks show geochemical affinity with a medium-K content, intermediate magmatic source. An origin from an active continental margin is suggested by the MORB normalized pattern of selected trace elements and dispersal of K_2O versus SiO_2 diagram.

(6) Geochemical affinity of the sandstones of the Bajo Barreal Formation with the Upper Cretaceous back-arc volcanic rocks assigned to the Divisadero Formation, outcropping along the Argentina-Chile border, suggest that they are the more probable source rocks. In addition, this inference is sustained by similar petrographic features, scarcity of basaltic intercalations and a similar REE pattern. However, a minor input of sediments from Ñirehuao Formation can not be rejected; although this unit has major proportion of layers with low silica content and this mafic contribution is not detected in the Bajo Barreal Formation sandstones.

(7) This study establishes, for the first time, a strong petrographic and geochemical correlation between the Late Cretaceous volcanic arc located in the western margin of South America and their eastward sedimentary counterpart (Bajo Barreal Formation, San Jorge Basin).

Acknowledgements

References

Amstrong-Altrin, J.S., Lee, Y.I., Verma, S.P., Ramasamy, S., 2004. Geochemistry of sandstones from the Upper Miocene Kudankulam Formation, southern India: implications for provenance, weathering, and tectonic setting. Journal of Sedimentary Research 74, 285–297.

Archangelsky, S., Bellosi, E., Jalfin, G., Perrot, C., 1994. Palynology and alluvial facies from the mid-Cretaceous of Patagonia, subsurface of San Jorge Basin. Cretaceous Research 15, 127–142.

Barcat, C., Cortiñas, J.S., Nevistic, V.A., Zucchi, H.E., 1989. Cuenca Golfo San Jorge. In: Chebli, G., Spalletti, L. (Eds.), Cuencas Sedimentarias Argentinas. Universidad Nacional de Tucumán, Tucumán, pp. 319–345.

Bathia, M.R., 1985. Rare earth element geochemistry of Australian Paleozoic greywackes and mudstones: provenance and tectonic control. Sedimentary Geology 45, 97–113.

Bellosi, E.S., 1995. Paleogeografía y cambios ambientales de la Patagonia central durante el Terciario Medio. Boletín de Informaciones Petroleras, Tercera Época 44, 50–83.

Bellosi, E.S., Sciutto, J.C., 2002. Laguna Palacios Formation (San Jorge Basin, Argentina): An Upper Cretaceous Loess-Paleosol Sequence from Central Patagonia. IX Reunión Argentina de Sedimentología. Asociación Argentina de Sedimentología, Córdoba, pp. 15.

Bellosi, E.S., González, M., Genise, J., 2002. Paleosuelos y sedimentación cretácica de la Cuenca San Jorge (Grupo Chubut) en la Sierra San Bernardo, Patagonia central. XV Congreso Geológico Argentino. Asociación Geológica Argentina, Calafate, pp. 747–753.

Best, M.G., Christiansen, E.H., 2001. Igneous Petrology. Blackwell Science, USA, pp. 458.

Boggs, S., 1992. Petrology of Sedimentary Rocks. Macmillian Publishing Company, New York, pp. 707.

Bridge, J.S., Jalfin, G.A., Georgieff, S.M., 2000. Geometry, lithofacies, and spatial distribution of Cretaceous fluvial sandstone bodies, San Jorge basin, Argentina: outcrop analog for the hydrocarbon-bearing Chubut Group. Journal of Sedimentary Research 70, 341–359.

Cembrano, J., Hervé, F., Lavenu, A., 1996. The Liquiñe-Ofqui fault zone: a long lived intra-arc fault system in southern Chile. Tectonophysics 259, 55–66.

Davies, D.K., Dienger, L., Selva, C., San Martín, H., 1994. Petrographic characteristics of productive and non-productive sandstones, Cañadón Minerales field, San Jorge Basin, Argentina. Society of Petroleum Engineers 27000, 1–6.

Dickinson, W.R., 1970. Interpreting detrital modes of graywacke and arkose. Journal of Sedimentary Petrology 40, 695–707.

Dickinson, W.R., Rich, E.I., 1972. Petrologic intervals and petrofacies in the Great Valley sequence, Sacramento valley, California. Geological Society of America Bulletin 83, 3007–3024.

Dickinson, W.R., Suczek, C.A., 1979. Plate tectonics and sandstone composition. American Association of Petroleum Geologists Bulletin 63, 2164–2182.

Dickinson, W.R., Beard, L.S., Brakenridge, G.R., Erjavec, J.L., Ferguson, R.C., Inman, K.F., Knepp, R.A., Lindberg, F.A., Ryberg, P.T., 1983. Provenance of North American Phanerozoic sandstones in relation to tectonic setting. Geological Society of America Bulletin 94, 222–235.

Dunn, T.L., Surdam, R.C., 1992. Diagenetic permeability heterogeneties of the Comodoro Rivadavia Formation. IV Reunión Argentina de Sedimentología. Asociación Argentina de Sedimentología, La Plata, pp. 209–215.

Estrada, E., 2002. Compactación mecánica y texturas de material infiltrado mecánicamente en la Formación Cañadón Seco (Cuenca del Golfo San Jorge). IX Reunión Argentina de Sedimentología. Asociación Argentina de Sedimentología, Córdoba, pp. 129.

Feruglio, E., 1949. Descripción geológica de la Patagonia. Dirección de Yacimientos Petrolíferos Fiscales, Buenos Aires, pp. 334.

Figari, E.G., Strelkov, E., Laffitte, G., Cid de La Paz, M.S., Courtade, S.F., Celaya, J., Vottero, A., Lafourcade, P., Martínez, R., Villar, H.J., 1999. Los sistemas petroleros de la Cuenca del Golfo San Jorge: síntesis estructural, estratigráfica y geoquímica. IV Congreso de Exploración y Desarrollo de Hidrocarburos. Instituto Argentino del Petróleo y del Gas, Mar del Plata, pp. 197–237.

Fisher, R.V., 1961. Proposed classification of volcaniclastic sediments and rocks. Geological Society of America Bulletin 72, 1409–1414.

Fisher, R.V., Schmincke, H.U., 1994. Volcaniclastic sediment transport and deposition. In: Pye, K. (Ed.), Sediment Transport and Depositional Processes. Blackwell, Cambridge, pp. 351–388.

Fitzgerald, M.G., Mitchum, R.M., Uliana, M.A., Biddle, K.T., 1990. Evolution of the San Jorge Basin, Argentina. American Association of Petroleum Geologists Bulletin 74, 879–920.

Folguera, A., Ramos, V.A., 2002. Los efectos producidos por la aproximación, colisión y subducción de dorsales pacíficas en los Andes Patagónicos. Acta Geológica Hispánica 37, 329–353.

Folguera, A., Iannizzotto, N.F., 2004. The Lagos La Plata and Fontana fold-and-thrust belt: long lived orogenesis at the edge of western Patagonia. Journal of South American Earth Sciences 16, 541–566.

Folk, R.L., 1974. Petrology of Sedimentary Rocks. Hemphill, Austin, pp. 182.

Folk, R.L., Andrews, P.B., Lewis, D.W., 1970. Detrital sedimentary rock classification and nomenclature for use in New Zealand. New Zealand Journal of Geology and Geophysics 13, 937–968.

Franzese, J., Spalletti, L., Gómez Pérez, I., Macdonald, D., 2003. Tectonic and paleoenvironmental evolution of Mesozoic sedimentary basins along the Andean foothills of Argentina (32°–54°). Journal of South American Earth Sciences 16, 81–90.

Genise, J.F., Sciutto, J.C., Laza, J.H., González, M.G., Bellosi, E.S., 2002. Fossil bee nests, coleopteran pupal chambers and tuffaceous paleosols from the Late Cretaceous Laguna Palacios Formation, Central Patagonia (Argentina). Palaeogeogrphy, Palaeoclimatology, Palaeoecology 177, 215–235.

Gilbert, J.S., Lane, S.J., 1994. The origin of accretionary lapilli. Bulletin of Volcanology 56, 398–411.

Gonzalez, M., Taboada, R., Stinco, L., 2002. Cuenca del Golfo San Jorge: los reservorios del flanco norte. In: Schiuma, M., Hinterwimmer, G., Vergani, G. (Eds.), Rocas Reservorio de las Cuencas Productivas de la Argentina. Instituto Argentino del Petróleo y del Gas, Mar del Plata, pp. 135–153.

Hechem, J.J., 1994. Modelo predictivo de reservorios en un sistema fluvial efímero del Chubutiano de la Cuenca del Golfo San Jorge, Argentina. Revista de la Asociación Argentina de Sedimentología 1, 3–14.

Hechem, J.J., 1998. Arquitectura y paleodrenaje del sistema fluvial efímero de la Formación Bajo Barreal, Cuenca del Golfo San Jorge, Argentina. Boletín de Informaciones Petroleras 53, 21–27.

Heiken, G., Wohletz, K., 1992. Volcanic Ash. University of California Press, Berkeley, pp. 246.

Hervé, F., Pankhurst, R.J., Fanning, C.M., Calderón, M., Yaxley, G.M., 2007. The South Patagonian Batholith: 150 my of granite magmatism on a plate margin. Lithos 97, 373–394.

Ingersoll, R.V., Bullard, T.F., Ford, R.L., Grimm, J.P., Pickle, J.D., Sares, S., 1984. The effect of grain size on detrital modes: a test of the Gazzi-Dickinson point-counting method. Journal of Sedimentary Petrology 54, 103–116.

Jalfin, G.A., Bellosi, E.S., Smith, E., Laffitte, G., 2002. Generación de petróleos y carga de reservorios en Manantiales Behr, Cuenca del Golfo San Jorge: un caso de exploración en áreas maduras. V Congreso de Exploración y Desarrollo de Hidrocarburos. Instituto Argentino del Petróleo y del Gas, Mar del Plata. CD edition.

Jalfin, G.A., Manceda, R., Palacio, L., Bellosi, E.S., Chebli, P., Coria, C., Miguel, K., Sanz, A., 2005. Caracterización de trampas y sellos de la Cuenca del Golfo San Jorge: esquema de compartimentación. In: Kozlowski, E., Vergani, G., Boll, A. (Eds.), Las Trampas de Hidrocarburos en las Cuencas Productivas de Argentina. Instituto Argentino del Petróleo y del Gas, Mar del Plata, pp. 415–450.

Legarreta, L., Uliana, M.A., 1994. Asociaciones de fósiles y hiatos en el Supra-cretácico-Neógeno de Patagonia: una perspectiva estratigráfico-secuencial. Ameghiniana 31, 257–281.

Le Maitre, R.W., Bateman, P., Dubek, A., Keller, J., Lameyre, J., Le Bas, M.J., Sabine, M.A., Schmid, R., Sorensen, H., Streckeisen, A., Woolley, A.R., Zanettin, B., 1989. A Classification of Igneous Rocks and Glossary of Terms: Recommendations of the International Union of Geological Sciences Subcommision on the Systematic of Igneous Rocks. Blackwell Scientific Publications, Oxford, pp. 193.

Lesta, P.J., 1968. Estratigrafía de la Cuenca del Golfo San Jorge. III Jornadas Geológicas Argentinas. Asociación Geológica Argentina, Buenos Aires, pp. 251–289.

Lesta, P., Ferello, R., 1972. Región extraandina de Chubut y norte de Santa Cruz. I Simposio de Geología Regional Argentina. Academia Nacional de Ciencias Córdoba, Córdoba. 601–653.

Mazzoni, M., 1986. Procesos y depósitos piroclásticos. Asociación Geológica Argentina, Buenos Aires, pp. 115.

McLennan, S.M., Hemming, S., McDaniel, D.K., Hanson, G.N., 1993. Geochemical approaches to sedimentation, provenance, and tectonics. Geological Society of America. Special Paper 284, 21–40.

McLennan, S.M., Bock, B., Hemming, S.R., Hurowitz, J.A., Lev, S.M., McDaniel, D.K., 2003. The roles of provenance and sedimentary processes in the geochemistry of sedimentary rocks. In: Lentz, D.R. (Ed.), Geochemistry of Sediments and Sedimentary Rocks: Evolutionary Considerations to Mineral Deposit-Forming Environments. Geological Association of Canada, GeoText, 4, pp. 7–38. Winnipeg.

Nesbitt, H.W., Young, G.M., 1982. Early Proterozoic climates and plate motions inferred from major element chemistry of lutites. Nature 299, 715–717.

Pankhurst, R.J., Leat, P.T., Sruoga, P., Rapela, C.W., Márquez, M., Storey, B.C., Riley, T.R., 1998. The Chon Aike province of Patagonia and related rocks in West Antarctica: a silicic large igneous province. Journal of Volcanology and Geothermal Research 81, 113–136.

Pankhurst, R.J., Weaver, S.D., Hervé, F., Larrondo, P., 1999. Mesozoic-Cenozoic evolution of the North Patagonian Batholith in Aysén, southern Chile. Journal of the Geological Society 156, 673–694.

Parada, M., Lahsen, A., Palacios, C., 2001. Ages and geochemistry of Mesozoic-Eocene back-arc volcanic rocks in the Aysén region of the Patagonian Andes, Chile. Revista Geológica de Chile 28, 25–46.

Paredes, J.M., Hudecek, N., Foix, N., Rodríguez, J.F., Nillni, A., 2003. Análisis paleo-ambiental de la Formación Matasiete (Aptiano) en su área tipo, noroeste de la Cuenca del Golfo San Jorge, Argentina. Revista de la Asociación Argentina de Sedimentología 10, 81–101.

Paredes, P., Foix, N., Colombo Piñol, F., Nillni, A., Allard, J.O., Marquillas, R.A., 2007. Volcanic and climatic controls on fluvial style in a high-energy system: the Lower Cretaceous Matasiete Formation, Golfo San Jorge basin, Argentina. Sedimentary Geology 202, 96–123.

Pearce, J.A., 1983. Role of the sub-continental lithosphere in magma genesis at active continental margins. In: Hawkesworth, C.J., Norry, M.J. (Eds.), Continental Basalts and Mantle Xenoliths. Shiva Publications, Nantwich, pp. 230–249.

Pearce, J.A., 1996. A user's guide to basalt discrimination diagrams. In: Wyman, D.A. (Ed.), Trace Element Geochemistry of Volcanic Rocks: Applications for Massive Sulphide Exploration. Geological Association of Canada, Winnipeg, pp. 79–114.

Peroni, G.O., Hegedus, A.G., Cerdan, J., Legarreta, L., Uliana, M.A., Laffitte, G., 1995. Hydrocarbon accumulation in an inverted segment of the Andean foreland: San Bernardo belt, central Patagonia. In: Tankard, A.J., Suárez, R., Welsink, H.J. (Eds.), Petroleoum Basins of South America. American Association of Petroleum Geologists Memoir, vol. 62, pp. 403–419. Tulsa.

Pittman, E.D., 1969. Destruction of plagioclase twins by stream transport. Journal of Sedimentary Petrology 33, 380–386.

Powers, M.C., 1953. A new roundness scale for sedimentary particles. Journal of Sedimentary Petrology 23, 117–119.

Ramos, V.A., 1976. Estratigrafía de los lagos Fontana y La Plata. I Congreso Geológico Chileno. Sociedad Geológica de Chile, Santiago, pp. 43–64.

Ramos, V.A., Kay, S.M., 1992. Southern Patagonian plateau basalts and deformation: backarc testimony of ridge collision. Tectonophysics 205, 261–282.

Richwood, P.C., 1989. Boundary lines within petrologic diagrams which use oxides of major and minor elements. Lithos 22, 247–263.

Rogers, A.F., Kerr, P.F., 1942. Optical Mineralogy, second ed. McGraw-Hill Book Company, New York and London, pp. 390.

Rolando, A.P., Hartmann, L.A., Santos, J.O.S., Fernández, R.R., Etchevery, R.O., Schalamuk, I.A., McNaughton, N.J., 2002. SHRIMP zircon U-Pb evidence for extended Mesozoic magmatism in the Patagonian Batholith and assimilation of Archean crustal components. Journal of South American Earth Sciences 15, 267–283.

Ronov, A.B., Balashov, Y.A., Girin, Y.P., Bratishko, R.K.H., Kazakov, G.A., 1974. Regularities of rare earth element distribution in the sedimentary shell and in the crust of the earth. Sedimentology 21, 171–193.

Roser, B.P., Korsch, R.J., 1988. Provenance signatures of sandstone-mudstone suites determined using discriminant function analysis of major-element data. Chemical Geology 67, 119–139.

Ryan, K.M., Williams, D.M., 2007. Testing the reliability of discrimination diagrams for determining the tectonic depositional environment of ancient sedimentary basins. Chemical Geology 242, 103–125.

Salomone, G., Biocca, M.I., Amoroso, A., Arocena, J.C., Ronanduano, G., Guerberoff, D., Palacio, L., 2002. Cuenca del Golfo San Jorge: los reservorios del flanco sur. In: Schiuma, M., Hinterwimmer, G., Vergani, G. (Eds.), Rocas Reservorio de las Cuencas Productivas de la Argentina. Instituto Argentino del Petróleo y del Gas, Mar del Plata, pp. 155–174.

Sanagua, J., Hlebszevitsch, J., Suárez, F., 2002. Cuenca del Golfo San Jorge: los reservorios del flanco oeste. In: Schiuma, M., Hinterwimmer, G., Vergani, G. (Eds.), Rocas Reservorio de las Cuencas Productivas de la Argentina. Instituto Argentino del Petróleo y del Gas, Mar del Plata, pp. 175–198.

Scasso, R.A., Limarino, C.O., 1997. Petrología y Diagénesis de Rocas Clásticas. Asociación Argentina de Sedimentología, Buenos Aires, pp. 257.

Schmid, R., 1981. Descriptive nomenclature and classification of pyroclastic deposits and fragments. Geologisches Rundschau 70, 794–799.

Sciutto, J.C., 1981. Geología del codo del río Senguerr, Chubut, Argentina. VIII Congreso Geológico Argentino. Asociación Geológica Argentina, San Luis, pp. 203–219.

Smith, G.A., 1988. Sedimentology of proximal to distal volcaniclastics dispersed across an active foldbelt: Ellensburg Formation (late Miocene), central Washington. Sedimentology 35, 953–977.

Smith, G.A., 1991. Facies sequences and geometries in continental volcaniclastic sediments. In: Fisher, R.V., Smith, G.A. (Eds.), Sedimentation in Volcanic Settings. Society for Sedimentary Geology Special Publication, 45, pp. 109–121. Tulsa.

Taylor, S.R., McLennan, S.M., 1985. The Continental Crust: Its Composition and Evolution. Blackwell, London, pp. 312.

Teruggi, M.E., 1962. Sobre la presencia de analcima sedimentaria en el Chubutiano del Codo del Senguerr. Revista del Museo de La Plata (nueva serie) Sección Geología 5, 193–217.

Teruggi, M.E., Rosetto, H., 1963. Petrología del Chubutiano del Codo Río Senguerr. Boletín de Informaciones Petroleras 1, 8–35.

Teruggi, M.E., Mazzoni, M.M., Spalletti, L.A., Andreis, R.R., 1978. Rocas Piroclásticas: Interpretación y Sistemática. Asociación Geológica Argentina, Buenos Aires, pp. 57.

Tófalo, O.R., Villalba, E., Chocan, E., 1992. Evaluación de la calidad como reservorio del tramo arenoso superior de la Formación Comodoro Rivadavia en el sector centro-oriental del yacimiento Pampa del Castillo, provincia de Chubut. IV Reunión Argentina de Sedimentología, La Plata, pp. 57–63.

Tunik, M.A., Vietto, M.E., Sciutto, J.C., Estrada, E., 2004. Procedencia de areniscas del Grupo Chubut en el área central de la Sierra de San Bernardo. Análisis preliminar. Revista de la Asociación Geológica Argentina 59, 601–606.

Uliana, M.A., Legarreta, L., Laffitte, G.A., Villar, H., 1999. Estratigrafía y geoquímica de las facies generadoras de hidrocarburos en las cuencas petrolíferas de Argentina. IV Congreso de Exploración y Desarrollo de Hidrocarburos. Instituto Argentino del Petróleo y del Gas, Mar del Plata, pp. 1–61.

Umazano, A.M., Visconti, G., Melchor, R.N., Bellosi, E.S., 2006. Petrography and provenance of Cretaceous fluvial sandstones of the Bajo Barreal Formation, San Jorge Basin, Argentina. IV Congreso Latinoamericano de Sedimentología y XI Reunión Argentina de Sedimentología. Asociación Argentina de Sedimentología, San Carlos de Bariloche, pp. 231.

Umazano, A.M., Bellosi, E., Visconti, G., Melchor, R.N., 2008. Mechanisms of aggradation in fluvial systems influenced by explosive volcanism: an example from the Late Cretaceous Bajo Barreal Formation, San Jorge Basin, Argentina. Sedimentary Geology 203, 213–228.

Wilson, M., 1989. Igneous Petrogenesis. Unwin Hyman, London, pp. 466.

Winchester, J.A., Floyd, P.A., 1977. Geochemical discrimination of different magma series and the differentiation products using immobile elements. Chemical Geology 20, 325–343.

Winter, J.D., 2001. An Introduction to Igneous and Metamorphic Petrology. Prentice Hall, New Jersey, pp. 697.